A Hybrid High-Order method for nonlinear elasticity *

Michele Botti, Daniele Di Pietro, Pierre Sochala

A Hybrid High-Order method for nonlinear elasticity*

Michele Botti[†1], Daniele A. Di Pietro[‡1], and Pierre Sochala[§2]

[1] University of Montpellier, Institut Montpelliérain Alexander Grothendieck, 34095 Montpellier, France
[2] Bureau de Recherches Géologiques et Minières, 45060 Orléans, France

June 15, 2017

Abstract

In this work we propose and analyze a novel Hybrid High-Order discretization of a class of (linear and) nonlinear elasticity models in the small deformation regime which are of common use in solid mechanics. The proposed method is valid in two and three space dimensions, it supports general meshes including polyhedral elements and nonmatching interfaces, enables arbitrary approximation order, and has a reduced cost thanks to the possibility of statically condensing a large subset of the unknowns for linearized versions of the problem. Additionally, the method satisfies a local principle of virtual work on each mesh element, with interface tractions that obey the law of action and reaction. A complete analysis covering very general stress-strain laws is carried out, and optimal error estimates are proved. Extensive numerical validation on model test problems is also provided on two types of nonlinear models.

1 Introduction

In this work we develop and analyze a novel Hybrid High-Order (HHO) method for a class of (linear and) nonlinear elasticity problems in the small deformation regime.

Let $\Omega \subset \mathbb{R}^d$, $d \in \{2,3\}$, denote a bounded connected open polyhedral domain with Lipschitz boundary $\Gamma := \partial\Omega$ and outward normal $\boldsymbol{n}$. We consider a body that occupies the region Ω and is subjected to a volumetric force field $\boldsymbol{f} \in L^2(\Omega;\mathbb{R}^d)$. For the sake of simplicity, we assume the body fixed on Γ (extensions to other standard boundary conditions are possible). The nonlinear elasticity problem consists in finding a vector-valued displacement field $\boldsymbol{u} : \Omega \to \mathbb{R}^d$ solution of

$$-\boldsymbol{\nabla}\cdot\boldsymbol{\sigma}(\cdot, \boldsymbol{\nabla}_{\rm s}\boldsymbol{u}) = \boldsymbol{f} \qquad \text{in } \Omega, \tag{1a}$$

$$\boldsymbol{u} = \boldsymbol{0} \qquad \text{on } \Gamma, \tag{1b}$$

where $\boldsymbol{\nabla}_{\rm s}$ denotes the symmetric gradient. The stress-strain law $\boldsymbol{\sigma} : \Omega \times \mathbb{R}^{d\times d}_{\rm sym} \to \mathbb{R}^{d\times d}_{\rm sym}$ is assumed to satisfy regularity requirements closely inspired by [23], including conditions on its growth, coercivity, and monotonicity; cf. Assumption 1 for a precise statement. Problem (1) is relevant, e.g., in modeling the mechanical behavior of soft materials [40] and metal alloys [36]. Examples of stress-strain laws of common use in the engineering practice are collected in Section 2.

The HHO discretization studied in this work is inspired by recent works on linear elasticity [17] (where HHO methods where originally introduced) and Leray–Lions operators [13, 14]. It hinges on degrees of freedom (DOFs) that are discontinuous polynomials of degree $k \geqslant 1$ on the mesh and on the mesh skeleton. Based on these DOFs, we reconstruct discrete counterparts of the symmetric gradient and of the displacement by solving local linear problems inside each mesh element. These reconstruction

*This work was partially funded by the Bureau de Recherches Géologiques et Minières. The work of M. Botti was partially supported by Labex NUMEV (ANR-10-LABX-20) ref. 2014-2-006. The work of D. A. Di Pietro was partially supported by *Agence Nationale de la Recherche* project ANR-15-CE40-0005.

† michele.botti@umontpellier.fr
‡ daniele.di-pietro@umontpellier.fr
§ p.sochala@brgm.fr

operators are used to formulate a local contribution composed of two terms: a consistency term inspired by the weak formulation of problem (1) with $\boldsymbol{\nabla}_{\rm s}$ replaced by its discrete counterpart, and a stabilization term penalizing cleverly designed face-based residuals. The resulting method has several advantageous features: (i) it is valid in arbitrary space dimension; (ii) it supports arbitrary polynomial orders $\geqslant 1$ on fairly general meshes including, e.g., polyhedral elements and nonmatching interfaces; (iii) it satisfies inside each mesh element a local principle of virtual work with numerical tractions that obey the law of action and reaction; (iv) it is (relatively) inexpensive thanks to the possibility of statically condensing a large subset of the unknowns for linearized versions of the problem (encountered, e.g., when solving the corresponding system of nonlinear algebraic equations by the Newton method). Additionally, as shown by the numerical tests of Section 6, the method is extremely robust with respect to strong nonlinearities.

In the context of structural mechanics, discretization methods supporting polyhedral meshes and nonconforming interfaces can be useful for several reasons including, e.g., the use of hanging nodes for contact [6, 41] and interface elasticity [28] problems, the simplicity in mesh refinement [38] and coarsening [2, 20] for adaptivity, and the greater robustness to mesh distorsion [10] and fracture [32]. The use of high-order methods, on the other hand, can classically accelerate the convergence in the presence of regular exact solutions or when combined with local mesh refinement. Over the last few years, several discretization schemes supporting polyhedral meshes and/or high-order have been proposed for the linear version of problem (1); a non-exhaustive list includes [3, 17–19, 37]. For the nonlinear version, the literature is more scarce. Conforming approximations on standard meshes have been considered in [26, 27], where the convergence analysis is carried out assuming regularity for the exact displacement field $\boldsymbol{u}$ and the constraint tensor $\boldsymbol{\sigma}(\cdot, \boldsymbol{\nabla}_{\rm s}\boldsymbol{u})$ beyond the minimal regularity required by the weak formulation. Discontinuous Galerkin methods on standard meshes have been considered in [35], where convergence is proved for $d = 2$ assuming $\boldsymbol{u} \in H^{m+1}(\Omega; \mathbb{R}^2)$ for some $m > 2$, and in [5], where convergence to minimal regularity solutions is proved for stress-strain functions similar to [4]. General meshes are considered, on the other hand, in [4], where the authors propose a low-order VEM method for problem (1). Therein, an energy-norm convergence estimate in h (with h denoting, as usual, the meshsize) is proved when $\boldsymbol{u} \in H^2(\Omega; \mathbb{R}^d)$ under the assumption that the function $\boldsymbol{\tau} \mapsto \boldsymbol{\sigma}(\cdot, \boldsymbol{\tau})$ is piecewise C^1 with positive definite and bounded differential inside each mesh element. These conditions on the stress-strain function are stronger than the ones considered in Assumption 13 to derive error estimates for our HHO method. Convergence to solutions that exhibit only the minimal regularity required by the weak formulation and for stress-strain functions as in Assumption 1 is proved in [23] for Gradient Schemes [22]. In this case, convergence rates are only proved for the linear case. We note, in passing, that the HHO method studied here fails to enter the Gradient Scheme framework essentially because the stabilization term cannot be embedded into the discrete symmetric gradient operator.

We carry out a complete analysis for the proposed HHO discretization of problem (1). Existence of a discrete solution is proved in Theorem 8, where we also identify a strict monotonicity assumption on the stress-strain law which ensures uniqueness. Convergence to minimal regularity solutions $\boldsymbol{u} \in H_0^1(\Omega; \mathbb{R}^d)$ is proved in Theorem 10 using a compactness argument inspired by [13, 23]. More precisely, we prove for monotone stress-strain laws that (i) the discrete displacement field strongly converges (up to a subsequence) to $\boldsymbol{u}$ in $L^q(\Omega; \mathbb{R}^d)$ with $1 \leqslant q < +\infty$ if $d = 2$ and $1 \leqslant q < 6$ if $d = 3$; (ii) the discrete strain tensor weakly converges (up to a subsequence) to $\boldsymbol{\nabla}_{\rm s}\boldsymbol{u}$ in $L^2(\Omega, \mathbb{R}^{d\times d})$. Notice that our results are slightly stronger than [23, Theorem 3.5] (cf. also Remark 3.6 therein) because the HHO discretization is compact as proved in Lemma 18. If, additionally, strict monotonicity holds for $\boldsymbol{\sigma}$, the strain tensor strongly converges and convergence extends to the whole sequence. An optimal energy-norm error estimate in h^{k+1} is then proved in Theorem 15 under the additional conditions of Lipschitz continuity and strong monotonicity on the stress-strain law; cf. Assumption 13. The performance of the method is investigated in Section 6 on a complete panel of model problems using stress-strain laws corresponding to real materials.

The rest of the paper is organized as follows. In Section 2 we formulate the assumptions on the stress-strain function $\boldsymbol{\sigma}$, provide several examples of models relevant in the engineering practice, and write the weak formulation of problem (1). In Section 3 we introduce the notation for the mesh and recall a few known results. In Section 4 we discuss the choice of DOFs, formulate the local reconstructions, and state the discrete problem along with the main results, collected in Theorems 8, 10, and 15. In Section 5 we show that the HHO method satisfies on each mesh element a discrete counterpart of the principle of virtual work, and that interface tractions obey the law of action and reaction. Section 6 contains numerical tests, while the proofs of the main results are given in Section 7. Finally, Appendix A contains the proofs of intermediate technical results. This structure allows different levels of reading. In particular, readers mainly interested in the numerical recipe and results may focus primarily on the material of Sections 2–6.

2 Setting and examples

For the stress-strain function, we make the following

Assumption 1 (Stress-strain function I)**.** The stress-strain function $\boldsymbol{\sigma} : \Omega \times \mathbb{R}^{d\times d}_{\rm sym} \to \mathbb{R}^{d\times d}_{\rm sym}$ is a Caratheodory function, namely

$$\boldsymbol{\sigma}(\boldsymbol{x},\cdot) \text{ is continuous on } \mathbb{R}^{d\times d}_{\rm sym} \text{ for a.e. } \boldsymbol{x}\in\Omega, \tag{2a}$$
$$\boldsymbol{\sigma}(\cdot,\boldsymbol{\tau}) \text{ is measurable on } \Omega \text{ for all } \boldsymbol{\tau}\in\mathbb{R}^{d\times d}_{\rm sym}, \tag{2b}$$

and it holds $\boldsymbol{\sigma}(\cdot,\boldsymbol{0}) \in L^2(\Omega;\mathbb{R}^{d\times d})$. Moreover, there exist real numbers $\overline{\sigma}$, $\underline{\sigma} \in (0,+\infty)$ such that, for a.e. $\boldsymbol{x}\in\Omega$, and all $\boldsymbol{\tau},\boldsymbol{\eta}\in\mathbb{R}^{d\times d}_{\rm sym}$, the following conditions hold:

$$\|\boldsymbol{\sigma}(\boldsymbol{x},\boldsymbol{\tau})-\boldsymbol{\sigma}(\boldsymbol{x},\boldsymbol{0})\|_{d\times d} \leqslant \overline{\sigma}\|\boldsymbol{\tau}\|_{d\times d}, \quad \text{(growth)} \tag{2c}$$
$$\boldsymbol{\sigma}(\boldsymbol{x},\boldsymbol{\tau}) : \boldsymbol{\tau} \geqslant \underline{\sigma}\|\boldsymbol{\tau}\|^2_{d\times d}, \quad \text{(coercivity)} \tag{2d}$$
$$(\boldsymbol{\sigma}(\boldsymbol{x},\boldsymbol{\tau})-\boldsymbol{\sigma}(\boldsymbol{x},\boldsymbol{\eta})) : (\boldsymbol{\tau}-\boldsymbol{\eta}) \geqslant 0, \quad \text{(monotonicity)} \tag{2e}$$

where $\boldsymbol{\tau}:\boldsymbol{\eta} := \sum_{i,j=1}^d \tau_{i,j}\eta_{i,j}$ and $\|\boldsymbol{\tau}\|^2_{d\times d} := \boldsymbol{\tau}:\boldsymbol{\tau}$.

We next discuss a number of meaningful models that satisfy the above assumptions.

Example 2 (Linear elasticity)**.** The linear elasticity model corresponds to

$$\boldsymbol{\sigma}(\cdot,\boldsymbol{\nabla}_{\rm s}\boldsymbol{u}) = \boldsymbol{C}(\cdot)\boldsymbol{\nabla}_{\rm s}\boldsymbol{u},$$

where $\boldsymbol{C}$ is a fourth order tensor. Being linear, the previous stress-strain relation clearly satisfies Assumption 1 provided that $\boldsymbol{C}$ is uniformly elliptic. A particular case of the previous stress-strain relation is the usual linear elasticity Cauchy stress tensor

$$\boldsymbol{\sigma}(\boldsymbol{\nabla}_{\rm s}\boldsymbol{u}) = \lambda\,\mathrm{tr}(\boldsymbol{\nabla}_{\rm s}\boldsymbol{u})\boldsymbol{I}_d + 2\mu\boldsymbol{\nabla}_{\rm s}\boldsymbol{u}, \tag{3}$$

where $\mathrm{tr}(\boldsymbol{\tau}) := \boldsymbol{\tau}:\boldsymbol{I}_d$ and $\lambda,\mu\in\mathbb{R}$ are Lamé's parameters.

Example 3 (Hencky–Mises model)**.** The nonlinear Hencky–Mises model of [27, 34] corresponds to the stress-strain relation

$$\boldsymbol{\sigma}(\boldsymbol{\nabla}_{\rm s}\boldsymbol{u}) = \tilde{\lambda}(\mathrm{dev}(\boldsymbol{\nabla}_{\rm s}\boldsymbol{u}))\,\mathrm{tr}(\boldsymbol{\nabla}_{\rm s}\boldsymbol{u})\boldsymbol{I}_d + 2\tilde{\mu}(\mathrm{dev}(\boldsymbol{\nabla}_{\rm s}\boldsymbol{u}))\boldsymbol{\nabla}_{\rm s}\boldsymbol{u}, \tag{4}$$

where $\tilde{\lambda}$ and $\tilde{\mu}$ are the nonlinear Lamé's scalar functions and $\mathrm{dev} : \mathbb{R}^{d\times d}_{\rm sym} \to \mathbb{R}$ defined by $\mathrm{dev}(\boldsymbol{\tau}) = \mathrm{tr}(\boldsymbol{\tau}^2) - \frac{1}{d}\,\mathrm{tr}(\boldsymbol{\tau})^2$ is the deviatoric operator. Conditions on $\tilde{\lambda}$ and $\tilde{\mu}$ such that $\boldsymbol{\sigma}$ satisfies Assumption 1 can be found in [1, 4].

Example 4 (An isotropic damage model)**.** The isotropic damage model of [9] corresponds to the stress-strain relation

$$\boldsymbol{\sigma}(\cdot,\boldsymbol{\nabla}_{\rm s}\boldsymbol{u}) = (1-D(\boldsymbol{\nabla}_{\rm s}\boldsymbol{u}))\boldsymbol{C}(\cdot)\boldsymbol{\nabla}_{\rm s}\boldsymbol{u}, \tag{5}$$

where $D : \mathbb{R}^{d\times d}_{\rm sym} \to \mathbb{R}$ is the scalar damage function. If there exists a continuous and bounded function $f : [0,+\infty) \to [a,b]$ for some $0 < a \leqslant b$, such that $s\in[0,+\infty) \to sf(s)$ is non-decreasing and, for all $\boldsymbol{\tau}\in\mathbb{R}^{d\times d}_{\rm sym}$, $D(\boldsymbol{\tau}) = 1 - f(|\boldsymbol{\tau}|)$, the damage model constitutive relation satisfies Assumption 1.

In the numerical experiments of Section 6 we will also consider the following model, relevant in engineering applications, which however does not satisfy Assumption 1 in general.

Example 5 (The second-order elasticity model)**.** The nonlinear second-order isotropic elasticity model of [12, 30, 31] corresponds to the stress-strain relation

$$\begin{aligned}\boldsymbol{\sigma}(\boldsymbol{\nabla}_{\mathrm{s}}\boldsymbol{u}) = \lambda\,\mathrm{tr}(\boldsymbol{\nabla}_{\mathrm{s}}\boldsymbol{u})\boldsymbol{I}_d + 2\mu\boldsymbol{\nabla}_{\mathrm{s}}\boldsymbol{u}\\ + B\,\mathrm{tr}((\boldsymbol{\nabla}_{\mathrm{s}}\boldsymbol{u})^2)\boldsymbol{I}_d + 2B\,\mathrm{tr}(\boldsymbol{\nabla}_{\mathrm{s}}\boldsymbol{u})\boldsymbol{\nabla}_{\mathrm{s}}\boldsymbol{u} + C\,\mathrm{tr}(\boldsymbol{\nabla}_{\mathrm{s}}\boldsymbol{u})^2\boldsymbol{I}_d + A(\boldsymbol{\nabla}_{\mathrm{s}}\boldsymbol{u})^2,\end{aligned} \quad (6)$$

where λ and μ are the standard Lamé's parameter, and $A, B, C \in \mathbb{R}$ are the second-order moduli.

Remark 6 (Energy density functions). Examples 2, 3, and 5, used in numerical tests of Section 6, can be interpreted in the framework of hyperelasticity. Hyperelasticity is a type of constitutive model for ideally elastic materials in which the stress-strain relation derives from a stored energy density function $\Psi : \mathbb{R}^{d\times d}_{\mathrm{sym}} \to \mathbb{R}$, namely

$$\boldsymbol{\sigma}(\boldsymbol{\tau}) := \frac{\partial\Psi(\boldsymbol{\tau})}{\partial\boldsymbol{\tau}}.$$

The stored energy density function leading to the linear Cauchy stress tensor (3) is

$$\Psi_{\mathrm{lin}}(\boldsymbol{\tau}) := \frac{\lambda}{2}\,\mathrm{tr}(\boldsymbol{\tau})^2 + \mu\,\mathrm{tr}(\boldsymbol{\tau}^2), \quad (7)$$

while, in the Hencky–Mises model (4), it is defined such that

$$\Psi_{\mathrm{hm}}(\boldsymbol{\tau}) := \frac{\alpha}{2}\,\mathrm{tr}(\boldsymbol{\tau})^2 + \Phi(\mathrm{dev}(\boldsymbol{\tau})). \quad (8)$$

Here $\alpha \in (0, +\infty)$, while $\Phi : [0, +\infty) \to \mathbb{R}$ is a function of class C^2 satisfying, for some positive constants C_1, C_2, and C_3,

$$C_1 \leqslant \Phi'(\rho) < \alpha \quad , \quad |\rho\Phi''(\rho)| \leqslant C_2 \quad \text{and} \quad \Phi'(\rho) + 2\rho\Phi''(\rho) \geqslant C_3 \quad \forall\rho \in [0, +\infty). \quad (9)$$

Deriving the energy density function (8) yields the stress-strain relation (4) with nonlinear Lamé's functions $\tilde{\mu}(\rho) := \Phi'(\rho)$ and $\tilde{\lambda}(\rho) := \alpha - \Phi'(\rho)$. Taking $\alpha = \lambda + \mu$ and $\Phi(\rho) = \mu\rho$ in (8) leads to the linear case. Finally, the second-order elasticity model (6) is obtained by adding third-order terms to the linear stored energy density function defined in (7):

$$\Psi_{\mathrm{snd}}(\boldsymbol{\tau}) := \frac{\lambda}{2}\,\mathrm{tr}(\boldsymbol{\tau})^2 + \mu\,\mathrm{tr}\left(\boldsymbol{\tau}^2\right) + \frac{C}{3}\,\mathrm{tr}(\boldsymbol{\tau})^3 + B\,\mathrm{tr}(\boldsymbol{\tau})\,\mathrm{tr}(\boldsymbol{\tau}^2) + \frac{A}{3}\,\mathrm{tr}(\boldsymbol{\tau}^3). \quad (10)$$

The weak formulation of problem (1) that will serve as a starting point for the development and analysis of the HHO method reads

$$\text{Find } \boldsymbol{u} \in H^1_0(\Omega;\mathbb{R}^d) \text{ such that } a(\boldsymbol{u},\boldsymbol{v}) = \int_\Omega \boldsymbol{f}\cdot\boldsymbol{v} \quad \forall\boldsymbol{v} \in H^1_0(\Omega;\mathbb{R}^d), \quad (11)$$

where $H^1_0(\Omega;\mathbb{R}^d)$ is the zero-trace subspace of $H^1(\Omega;\mathbb{R}^d)$ and the function $a : H^1_0(\Omega;\mathbb{R}^d)\times H^1_0(\Omega;\mathbb{R}^d) \to \mathbb{R}$ is such that

$$a(\boldsymbol{v},\boldsymbol{w}) := \int_\Omega \boldsymbol{\sigma}(\boldsymbol{x},\boldsymbol{\nabla}_{\mathrm{s}}\boldsymbol{v}(\boldsymbol{x})) : \boldsymbol{\nabla}_{\mathrm{s}}\boldsymbol{w}(\boldsymbol{x})\mathrm{d}\boldsymbol{x}.$$

Throughout the rest of the paper, to alleviate the notation, we omit the dependence on the space variable $\boldsymbol{x}$ and the differential $\mathrm{d}\boldsymbol{x}$ from integrals.

3 Notation and basic results

Denote by $\mathcal{H} \subset \mathbb{R}^+_*$ a countable set of meshsizes having 0 as its unique accumulation point. We consider refined mesh sequences $(\mathcal{T}_h)_{h\in\mathcal{H}}$ where each $\mathcal{T}_h$ is a finite collection of nonempty disjoint open polyhedral elements T with boundary ∂T such that $\overline{\Omega} = \bigcup_{T\in\mathcal{T}_h}\overline{T}$ and $h = \max_{T\in\mathcal{T}_h} h_T$ with

h_T diameter of T. We assume that mesh regularity holds in the sense of [16, Definition 1.38], i.e., for all $h \in \mathcal{H}$, $\mathcal{T}_h$ admits a matching simplicial submesh $\mathfrak{T}_h$ and there exists a real number $\varrho > 0$ independent of h such that, for all $h \in \mathcal{H}$, (i) for all simplex $S \in \mathfrak{T}_h$ of diameter h_S and inradius r_S, $\varrho h_S \leqslant r_S$ and (ii) for all $T \in \mathcal{T}_h$ and all $S \in \mathfrak{T}_h$ such that $S \subset T$, $\varrho h_T \leqslant h_S$.

We define a face F as a hyperplanar closed connected subset of $\overline{\Omega}$ with positive $(d-1)$-dimensional Hausdorff measure such that (i) either there exist distinct $T_1, T_2 \in \mathcal{T}_h$ such that $F \subset \partial T_1 \cap \partial T_2$ and F is called an interface or (ii) there exists $T \in \mathcal{T}_h$ such that $F \subset \partial T \cap \Gamma$ and F is called a boundary face. Interfaces are collected in the set $\mathcal{F}_h^{\rm i}$, boundary faces in $\mathcal{F}_h^{\rm b}$, and we let $\mathcal{F}_h := \mathcal{F}_h^{\rm i} \cup \mathcal{F}_h^{\rm b}$. For all $T \in \mathcal{T}_h$, $\mathcal{F}_T := \{F \in \mathcal{F}_h \mid F \subset \partial T\}$ denotes the set of faces contained in ∂T and, for all $F \in \mathcal{F}_T$, $\boldsymbol{n}_{TF}$ is the unit normal to F pointing out of T.

Let X be a mesh element or face. For an integer $l \geqslant 0$, we denote by $\mathbb{P}^l(X;\mathbb{R})$ the space spanned by the restriction to X of scalar-valued, d-variate polynomials of total degree l. The L^2-projector $\pi_X^l : L^1(X;\mathbb{R}) \to \mathbb{P}^l(X;\mathbb{R})$ is defined such that, for all $v \in L^1(X;\mathbb{R})$,

$$\int_X (\pi_X^l v - v) = 0 \qquad \forall w \in \mathbb{P}^l(X;\mathbb{R}). \tag{12}$$

When dealing with the vector-valued polynomial space $\mathbb{P}^l(X;\mathbb{R}^d)$ or with the tensor-valued polynomial space $\mathbb{P}^l(X;\mathbb{R}^{d\times d})$, we use the boldface notation $\boldsymbol{\pi}_X^l$ for the corresponding L^2-orthogonal projectors acting component-wise.

On regular mesh sequences, we have the following optimal approximation properties for π_T^l (for a proof, cf. [16, Lemmas 1.58 and 1.59] and, in a more general framework, [14, Lemmas 3.4 and 3.6]): There exists a real number $C_{\rm app} > 0$ such that, for all $s \in \{1, \ldots, l+1\}$, all $h \in \mathcal{H}$, all $T \in \mathcal{T}_h$, and all $v \in H^s(T;\mathbb{R})$,

$$|v - \pi_T^l v|_{H^m(T;\mathbb{R})} \leqslant C_{\rm app} h_T^{s-m} |v|_{H^s(T;\mathbb{R})} \qquad \forall m \in \{0, \ldots, s\}, \tag{13a}$$

$$|v - \pi_T^l v|_{H^m(\mathcal{F}_T;\mathbb{R})} \leqslant C_{\rm app} h_T^{s-m-\frac{1}{2}} |v|_{H^s(T;\mathbb{R})} \qquad \forall m \in \{0, \ldots, s-1\}. \tag{13b}$$

Other useful geometric and functional analytic results on regular mesh sequences can be found in [16, Chapter 1] and [13, 14].

At the global level, we define broken versions of polynomial and Sobolev spaces. In particular, for an integer $l \geqslant 0$, we denote by $\mathbb{P}^l(\mathcal{T}_h;\mathbb{R})$, $\mathbb{P}^l(\mathcal{T}_h;\mathbb{R}^d)$, and $\mathbb{P}^l(\mathcal{T}_h;\mathbb{R}^{d\times d})$, respectively, the space of scalar-valued, vector-valued, and tensor-valued broken polynomial functions on $\mathcal{T}_h$ of total degree l. The space of broken vector-valued polynomial functions of total degree l on the trace of the mesh on the domain boundary Γ is denoted by $\mathbb{P}^l(\mathcal{F}_h^{\rm b};\mathbb{R}^d)$. Similarly, for an integer $s \geqslant 1$, $H^s(\mathcal{T}_h;\mathbb{R})$, $H^s(\mathcal{T}_h;\mathbb{R}^d)$, and $H^s(\mathcal{T}_h;\mathbb{R}^{d\times d})$ are the scalar-valued, vector-valued, and tensor-valued broken Sobolev spaces of index s.

Throughout the rest of the paper, for $X \subset \overline{\Omega}$, we denote by $\|\cdot\|_X$ the standard norm in $L^2(X;\mathbb{R})$, with the convention that the subscript is omitted whenever $X = \Omega$. The same notation is used for the vector- and tensor-valued spaces $L^2(X;\mathbb{R}^d)$ and $L^2(X;\mathbb{R}^{d\times d})$.

4 The Hybrid High-Order method

In this section we define the space of DOFs and the local reconstructions, and we state the discrete problem along with the main results (whose proof is postponed to Section 7).

4.1 Degrees of freedom

Let a polynomial degree $k \geqslant 1$ be fixed. The DOFs for the displacement are collected in the space

$$\underline{\boldsymbol{U}}_h^k := \left(\bigtimes_{T\in\mathcal{T}_h} \mathbb{P}^k(T;\mathbb{R}^d) \right) \times \left(\bigtimes_{F\in\mathcal{F}_h} \mathbb{P}^k(F;\mathbb{R}^d) \right),$$

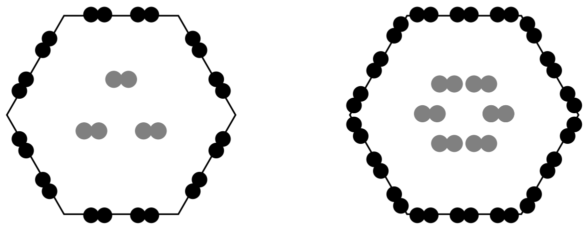

Figure 1: Local DOFs for $k = 1$ (left) and $k = 2$ (right). Shaded DOFs can be locally eliminated by static condensation when solving linearized versions of problem (24).

see Figure 1. For a generic collection of DOFs in $\underline{\boldsymbol{U}}_h^k$, we use the notation $\underline{\boldsymbol{v}}_h := \big((\boldsymbol{v}_T)_{T\in\mathcal{T}_h}, (\boldsymbol{v}_F)_{F\in\mathcal{F}_h}\big)$. We also denote by $\boldsymbol{v}_h \in \mathbb{P}^k(\mathcal{T}_h;\mathbb{R}^d)$ and $\boldsymbol{v}_{\Gamma,h} \in \mathbb{P}^k(\mathcal{F}_h^{\mathrm{b}};\mathbb{R}^d)$ (not underlined) the broken polynomial functions such that

$$(\boldsymbol{v}_h)_{|T} = \boldsymbol{v}_T \quad \forall T \in \mathcal{T}_h \qquad \text{and} \qquad (\boldsymbol{v}_{\Gamma,h})_{|F} = \boldsymbol{v}_F \quad \forall F \in \mathcal{F}_h^{\mathrm{b}}.$$

The restrictions of $\underline{\boldsymbol{U}}_h^k$ and $\underline{\boldsymbol{v}}_h$ to a mesh element T are denoted by $\underline{\boldsymbol{U}}_T^k$ and $\underline{\boldsymbol{v}}_T = \big(\boldsymbol{v}_T, (\boldsymbol{v}_F)_{F\in\mathcal{F}_T}\big)$, respectively. The space $\underline{\boldsymbol{U}}_h^k$ is equipped with the following discrete strain semi-norm:

$$\|\underline{\boldsymbol{v}}_h\|_{\epsilon,h} := \left(\sum_{T\in\mathcal{T}_h} \|\underline{\boldsymbol{v}}_h\|_{\epsilon,T}^2\right)^{1/2}, \qquad \|\underline{\boldsymbol{v}}_h\|_{\epsilon,T}^2 := \|\boldsymbol{\nabla}_{\mathrm{s}}\boldsymbol{v}_T\|_T^2 + \sum_{F\in\mathcal{F}_T} h_F^{-1}\|\boldsymbol{v}_F - \boldsymbol{v}_T\|_F^2. \tag{14}$$

The DOFs corresponding to a given function $\boldsymbol{v} \in H^1(\Omega;\mathbb{R}^d)$ are obtained by means of the reduction map $\underline{\boldsymbol{I}}_h^k : H^1(\Omega;\mathbb{R}^d) \to \underline{\boldsymbol{U}}_h^k$ such that

$$\underline{\boldsymbol{I}}_h^k\boldsymbol{v} := \big((\boldsymbol{\pi}_T^k\boldsymbol{v})_{T\in\mathcal{T}_h}, (\boldsymbol{\pi}_F^k\boldsymbol{v})_{F\in\mathcal{F}_h}\big), \tag{15}$$

where we remind the reader that $\boldsymbol{\pi}_T^k$ and $\boldsymbol{\pi}_F^k$ denote the L^2-orthogonal projectors on $\mathbb{P}^k(T;\mathbb{R}^d)$ and $\mathbb{P}^k(F;\mathbb{R}^d)$, respectively. For all mesh elements $T \in \mathcal{T}_h$, the local reduction map $\underline{\boldsymbol{I}}_T^k : H^1(T;\mathbb{R}^d) \to \underline{\boldsymbol{U}}_T^k$ is obtained by a restriction of $\underline{\boldsymbol{I}}_h^k$, and is therefore such that for all $\boldsymbol{v} \in H^1(T;\mathbb{R}^d)$

$$\underline{\boldsymbol{I}}_T^k\boldsymbol{v} = \big(\boldsymbol{\pi}_T^k\boldsymbol{v}, (\boldsymbol{\pi}_F^k\boldsymbol{v})_{F\in\mathcal{F}_T}\big). \tag{16}$$

4.2 Local reconstructions

We introduce symmetric gradient and displacement reconstruction operators devised at the element level that are instrumental in the formulation of the method.

Let a mesh element $T \in \mathcal{T}_h$ be fixed. The local symmetric gradient reconstruction operator $\boldsymbol{G}_{\mathrm{s},T}^k : \underline{\boldsymbol{U}}_T^k \to \mathbb{P}^k(T;\mathbb{R}^{d\times d}_{\mathrm{sym}})$ is obtained by solving the following pure traction problem: For a given local collection of DOFs $\underline{\boldsymbol{v}}_T = \big(\boldsymbol{v}_T, (\boldsymbol{v}_F)_{F\in\mathcal{F}_T}\big) \in \underline{\boldsymbol{U}}_T^k$, find $\boldsymbol{G}_{\mathrm{s},T}^k\underline{\boldsymbol{v}}_T \in \mathbb{P}^k(T;\mathbb{R}^{d\times d}_{\mathrm{sym}})$ such that, for all $\boldsymbol{\tau} \in \mathbb{P}^k(T;\mathbb{R}^{d\times d}_{\mathrm{sym}})$,

$$\int_T \boldsymbol{G}_{\mathrm{s},T}^k\underline{\boldsymbol{v}}_T : \boldsymbol{\tau} = -\int_T \boldsymbol{v}_T\cdot(\boldsymbol{\nabla}\cdot\boldsymbol{\tau}) + \sum_{F\in\mathcal{F}_T}\int_F \boldsymbol{v}_F\cdot(\boldsymbol{\tau}\boldsymbol{n}_{TF}) \tag{17a}$$

$$= \int_T \boldsymbol{\nabla}_{\mathrm{s}}\boldsymbol{v}_T : \boldsymbol{\tau} + \sum_{F\in\mathcal{F}_T}\int_F (\boldsymbol{v}_F - \boldsymbol{v}_T)\cdot(\boldsymbol{\tau}\boldsymbol{n}_{TF}). \tag{17b}$$

The right-hand side of (17a) is designed to resemble an integration by parts formula where the role of the function represented by the DOFs in $\underline{\boldsymbol{v}}_T$ is played by $\boldsymbol{v}_T$ inside the volumetric integral and by $(\boldsymbol{v}_F)_{F\in\mathcal{F}_T}$ inside boundary integrals. The reformulation (17b), obtained integrating by parts the first term in the right-hand side of (17a), highlights the fact that our method is nonconforming, as the second addend accounts for the difference between $\boldsymbol{v}_F$ and $\boldsymbol{v}_T$.

The definition of the symmetric gradient reconstruction is justified observing that, using the definitions (16) of the local reduction map $\underline{\boldsymbol{I}}_T^k$ and (12) of the L^2-orthogonal projectors $\boldsymbol{\pi}_T^k$ and $\boldsymbol{\pi}_F^k$ in (17a), one can prove the following commuting property: For all $T \in \mathcal{T}_h$ and all $\boldsymbol{v} \in H^1(T;\mathbb{R}^d)$,

$$\boldsymbol{G}_{\mathrm{s},T}^k \underline{\boldsymbol{I}}_T^k \boldsymbol{v} = \boldsymbol{\pi}_T^k(\boldsymbol{\nabla}_{\mathrm{s}} \boldsymbol{v}). \tag{18}$$

As a result of (18) and (13), $\boldsymbol{G}_{\mathrm{s},T}^k \underline{\boldsymbol{I}}_T^k$ has optimal approximation properties in $\mathbb{P}^k(T;\mathbb{R}_{\mathrm{sym}}^{d\times d})$.

From $\boldsymbol{G}_{\mathrm{s},T}^k$, one can define the local displacement reconstruction operator $\boldsymbol{r}_T^{k+1} : \underline{\boldsymbol{U}}_T^k \to \mathbb{P}^{k+1}(T;\mathbb{R}^d)$ such that, for all $\underline{\boldsymbol{v}}_T \in \underline{\boldsymbol{U}}_T^k$, $\boldsymbol{\nabla}_{\mathrm{s}} \boldsymbol{r}_T^{k+1} \underline{\boldsymbol{v}}_T$ is the orthogonal projection of $\boldsymbol{G}_{\mathrm{s},T}^k \underline{\boldsymbol{v}}_T$ on $\boldsymbol{\nabla}_{\mathrm{s}} \mathbb{P}^{k+1}(T;\mathbb{R}^d) \subset \mathbb{P}^k(T;\mathbb{R}_{\mathrm{sym}}^{d\times d})$ and rigid-body motions are prescribed according to [17, Eq. (15)]. More precisely, we let $\boldsymbol{r}_T^{k+1} \underline{\boldsymbol{v}}_T$ be such that for all $\boldsymbol{w} \in \mathbb{P}^{k+1}(T;\mathbb{R}^d)$ it holds

$$\int_T (\boldsymbol{\nabla}_{\mathrm{s}} \boldsymbol{r}_T^{k+1} \underline{\boldsymbol{v}}_T - \boldsymbol{G}_{\mathrm{s},T}^k \underline{\boldsymbol{v}}_T) : \boldsymbol{\nabla}_{\mathrm{s}} \boldsymbol{w} = 0$$

and, denoting by $\boldsymbol{\nabla}_{\mathrm{ss}}$ the skew-symmetric part of the gradient operator, we have

$$\int_T \boldsymbol{r}_T^{k+1} \underline{\boldsymbol{v}}_T = \int_T \boldsymbol{v}_T, \qquad \int_T \boldsymbol{\nabla}_{\mathrm{ss}} \boldsymbol{r}_T^{k+1} \underline{\boldsymbol{v}}_T = \sum_{F \in \mathcal{F}_T} \int_F \frac{1}{2} \left(\boldsymbol{n}_{TF} \otimes \boldsymbol{v}_F - \boldsymbol{v}_F \otimes \boldsymbol{n}_{TF} \right).$$

Notice that, for a given $\underline{\boldsymbol{v}}_T \in \underline{\boldsymbol{U}}_T^k$, the displacement reconstruction $\boldsymbol{r}_T^{k+1} \underline{\boldsymbol{v}}_T$ is a vector-valued polynomial function one degree higher than the element-based DOFs $\boldsymbol{v}_T$. It was proved in [17, Lemma 2] that $\boldsymbol{r}_T^{k+1} \underline{\boldsymbol{I}}_T^k$ has optimal approximation properties in $\mathbb{P}^{k+1}(T;\mathbb{R}^d)$.

In what follows, we will also need the global counterparts of the discrete gradient and displacement operators $\boldsymbol{G}_{\mathrm{s},h}^k : \underline{\boldsymbol{U}}_h^k \to \mathbb{P}^k(\mathcal{T}_h;\mathbb{R}_{\mathrm{sym}}^{d\times d})$ and $\boldsymbol{r}_h^{k+1} : \underline{\boldsymbol{U}}_h^k \to \mathbb{P}^{k+1}(\mathcal{T}_h;\mathbb{R}^d)$ defined setting, for all $\underline{\boldsymbol{v}}_h \in \underline{\boldsymbol{U}}_h^k$ and all $T \in \mathcal{T}_h$,

$$(\boldsymbol{G}_{\mathrm{s},h}^k \underline{\boldsymbol{v}}_h)_{|T} = \boldsymbol{G}_{\mathrm{s},T}^k \underline{\boldsymbol{v}}_T, \qquad (\boldsymbol{r}_h^{k+1} \underline{\boldsymbol{v}}_h)_{|T} = \boldsymbol{r}_T^{k+1} \underline{\boldsymbol{v}}_T \tag{19}$$

The following consistency properties for $\boldsymbol{G}_{\mathrm{s},h}^k$ play a fundamental role in the convergence analysis carried out in Section 7.

Proposition 7 (Consistency of the discrete symmetric gradient operator)**.** *Let $(\mathcal{T}_h)_{h\in\mathcal{H}}$ be a regular mesh sequence, and let $\boldsymbol{G}_{\mathrm{s},h}^k$ be as in (19) with $\boldsymbol{G}_{\mathrm{s},T}^k$ defined by (17) for all $T \in \mathcal{T}_h$.*

1) Strong consistency. *For all $\boldsymbol{v} \in H^1(\Omega;\mathbb{R}^d)$ with $\underline{\boldsymbol{I}}_h^k$ defined by (15), it holds as $h \to 0$*

$$\boldsymbol{G}_{\mathrm{s},h}^k \underline{\boldsymbol{I}}_h^k \boldsymbol{v} \to \boldsymbol{\nabla}_{\mathrm{s}} \boldsymbol{v} \text{ strongly in } L^2(\Omega;\mathbb{R}^{d\times d}). \tag{20}$$

2) Sequential consistency. *For all $h \in \mathcal{H}$, define the discrete integration by parts residual $\mathcal{R}_h : \underline{\boldsymbol{U}}_h^k \times H^1(\Omega;\mathbb{R}_{\mathrm{sym}}^{d\times d}) \to \mathbb{R}$ such that, for all $\underline{\boldsymbol{v}}_h \in \underline{\boldsymbol{U}}_h^k$ and all $\boldsymbol{\tau} \in H^1(\Omega;\mathbb{R}_{\mathrm{sym}}^{d\times d})$,*

$$\mathcal{R}_h(\underline{\boldsymbol{v}}_h, \boldsymbol{\tau}) := \left| \int_\Omega \boldsymbol{G}_{\mathrm{s},h}^k \underline{\boldsymbol{v}}_h : \boldsymbol{\tau} - \int_\Gamma \boldsymbol{v}_{\Gamma,h} \cdot \boldsymbol{\gamma}_{\boldsymbol{n}}(\boldsymbol{\tau}) + \int_\Omega \boldsymbol{v}_h \cdot (\boldsymbol{\nabla} \cdot \boldsymbol{\tau}) \right|, \tag{21}$$

where $\boldsymbol{\gamma}_{\boldsymbol{n}}(\boldsymbol{\tau})$ is the normal trace of $\boldsymbol{\tau}$. Then, for all $\boldsymbol{\tau} \in H^1(\Omega;\mathbb{R}_{\mathrm{sym}}^{d\times d})$,

$$\lim_{h\to 0} \left(\max_{\underline{\boldsymbol{v}}_h \in \underline{\boldsymbol{U}}_h^k,\, \|\underline{\boldsymbol{v}}_h\|_{\epsilon,h}=1} \mathcal{R}_h(\underline{\boldsymbol{v}}_h, \boldsymbol{\tau}) \right) = 0. \tag{22}$$

Proof. See Appendix A.1. □

4.3 Discrete problem

We define the following subspace of $\underline{\boldsymbol{U}}_h^k$ strongly accounting for the homogeneous Dirichlet boundary condition (1b):

$$\underline{\boldsymbol{U}}_{h,0}^k := \left\{ \underline{\boldsymbol{v}}_h \in \underline{\boldsymbol{U}}_h^k \mid \boldsymbol{v}_F = \boldsymbol{0} \quad \forall F \in \mathcal{F}_h^{\mathrm{b}} \right\}, \tag{23}$$

and we notice that the map $\|\cdot\|_{\epsilon,h}$ defined by (14) is a norm on $\underline{\boldsymbol{U}}_{h,0}^k$. The HHO approximation of problem (11) reads:

$$\text{Find } \underline{\boldsymbol{u}}_h \in \underline{\boldsymbol{U}}_{h,0}^k \text{ such that } a_h(\underline{\boldsymbol{u}}_h, \underline{\boldsymbol{v}}_h) := A_h(\underline{\boldsymbol{u}}_h, \underline{\boldsymbol{v}}_h) + s_h(\underline{\boldsymbol{u}}_h, \underline{\boldsymbol{v}}_h) = \int_\Omega \boldsymbol{f} \cdot \boldsymbol{v}_h \quad \forall \underline{\boldsymbol{v}}_h \in \underline{\boldsymbol{U}}_{h,0}^k, \tag{24}$$

where the consistency contribution $A_h : \underline{\boldsymbol{U}}_h^k \times \underline{\boldsymbol{U}}_h^k \to \mathbb{R}$ and the stability contribution $s_h : \underline{\boldsymbol{U}}_h^k \times \underline{\boldsymbol{U}}_h^k \to \mathbb{R}$ are respectively defined setting

$$A_h(\underline{\boldsymbol{u}}_h, \underline{\boldsymbol{v}}_h) := \int_\Omega \boldsymbol{\sigma}(\cdot, \boldsymbol{G}_{\mathrm{s},h}^k \underline{\boldsymbol{u}}_h) : \boldsymbol{G}_{\mathrm{s},h}^k \underline{\boldsymbol{v}}_h, \tag{25}$$

$$s_h(\underline{\boldsymbol{u}}_h, \underline{\boldsymbol{v}}_h) := \sum_{T \in \mathcal{T}_h} s_T(\underline{\boldsymbol{u}}_T, \underline{\boldsymbol{v}}_T), \quad \text{with} \quad s_T(\underline{\boldsymbol{u}}_T, \underline{\boldsymbol{v}}_T) := \frac{\gamma}{h_F} \int_F \boldsymbol{\Delta}_{TF}^k \underline{\boldsymbol{u}}_T \cdot \boldsymbol{\Delta}_{TF}^k \underline{\boldsymbol{v}}_T. \tag{26}$$

A possible choice for the user dependent scaling parameter $\gamma > 0$ in (26) is $\gamma = \overline{\sigma}$. In s_T, we penalize in a least-square sense the face-based residual $\boldsymbol{\Delta}_{TF}^k : \underline{\boldsymbol{U}}_T^k \to \mathbb{P}^k(F; \mathbb{R}^d)$ such that, for all $T \in \mathcal{T}_h$, all $\underline{\boldsymbol{v}}_T \in \underline{\boldsymbol{U}}_T^k$, and all $F \in \mathcal{F}_T$,

$$\boldsymbol{\Delta}_{TF}^k \underline{\boldsymbol{v}}_T := \boldsymbol{\pi}_F^k(\boldsymbol{r}_T^{k+1} \underline{\boldsymbol{v}}_T - \boldsymbol{v}_F) - \boldsymbol{\pi}_T^k(\boldsymbol{r}_T^{k+1} \underline{\boldsymbol{v}}_T - \boldsymbol{v}_T). \tag{27}$$

This particular choice ensures that $\boldsymbol{\Delta}_{TF}^k$ vanishes whenever its argument is of the form $\underline{\boldsymbol{I}}_T^k \boldsymbol{w}$ with $\boldsymbol{w} \in \mathbb{P}^{k+1}(T; \mathbb{R}^d)$, a crucial property to obtain an energy-norm error estimate in h^{k+1}; cf. Theorem 15. Additionally, s_h is stabilizing in the sense that the following uniform norm equivalence holds (the proof is a straightforward modification of [17, Lemma 4]; cf. also Corollary 6 therein): There exists a real number $\eta > 0$ independent of h such that, for all $\underline{\boldsymbol{v}}_h \in \underline{\boldsymbol{U}}_{h,0}^k$,

$$\eta^{-1} \|\underline{\boldsymbol{v}}_h\|_{\epsilon,h}^2 \leqslant \|\boldsymbol{G}_{\mathrm{s},h}^k \underline{\boldsymbol{v}}_h\|^2 + s_h(\underline{\boldsymbol{v}}_h, \underline{\boldsymbol{v}}_h) \leqslant \eta \|\underline{\boldsymbol{v}}_h\|_{\epsilon,h}^2. \tag{28}$$

By (2d), this implies the coercivity of a_h.

4.4 Main results

In this section we collect the main results of this paper. The proofs are postponed to Section 7. We start by discussing existence and uniqueness of the discrete solution.

Theorem 8 (Existence and uniqueness of a discrete solution)**.** *Let Assumption 1 hold and let $(\mathcal{T}_h)_{h \in \mathcal{H}}$ be a regular mesh sequence. Then, for all $h \in \mathcal{H}$, there exists at least one solution $\underline{\boldsymbol{u}}_h \in \underline{\boldsymbol{U}}_{h,0}^k$ to problem (24). Additionally, if the stress-strain function $\boldsymbol{\sigma}$ is strictly monotone (i.e., if the inequality in (2e) is strict for $\boldsymbol{\tau} \neq \boldsymbol{\eta}$), the solution is unique.*

Proof. See Section 7.1. □

Remark 9 (Strict monotonicity of the stress-strain function). The strict monotonicity assumption is fulfilled, e.g., by the Hencky–Mises model (4) and by the damage model (5) when $D(\boldsymbol{\tau}) = 1 - f(|\boldsymbol{\tau}|)$, with f continuous, bounded, and such that $[0, +\infty) \ni s \mapsto sf(s)$ is strictly increasing. We observe, in passing, that the strict monotonicity is weaker than the strong monotonicity (30b) used in Theorem 15 to prove error estimates.

We then consider the convergence to solutions that only exhibit the minimal regularity required by the variational formulation (11).

Theorem 10 (Convergence)**.** *Let Assumption 1 hold, let $k \geqslant 1$, and let $(\mathcal{T}_h)_{h\in\mathcal{H}}$ be a regular mesh sequence. Further assume the existence of a real number $C_{\rm K} > 0$ depending on Ω, ϱ, and on k but independent of h such that, for all $\underline{\boldsymbol{v}}_h \in \underline{\boldsymbol{U}}_{h,0}^k$,*

$$\|\boldsymbol{v}_h\| + \|\boldsymbol{\nabla}_h \boldsymbol{v}_h\| \leqslant C_{\rm K} \|\underline{\boldsymbol{v}}_h\|_{\epsilon,h}, \tag{29}$$

where $\boldsymbol{\nabla}_h$ denotes the broken gradient on $H^1(\mathcal{T}_h;\mathbb{R}^d)$. For all $h \in \mathcal{H}$, let $\underline{\boldsymbol{u}}_h \in \underline{\boldsymbol{U}}_{h,0}^k$ be a solution to the discrete problem (24) on $\mathcal{T}_h$. Then, for all q such that $1 \leqslant q < +\infty$ if $d = 2$ or $1 \leqslant q < 6$ if $d = 3$, as $h \to 0$, up to a subsequence,

- *$\boldsymbol{u}_h \to \boldsymbol{u}$ strongly in $L^q(\Omega;\mathbb{R}^d)$,*
- *$\boldsymbol{G}_{{\rm s},h}^k \underline{\boldsymbol{u}}_h \to \boldsymbol{\nabla}_{\rm s}\boldsymbol{u}$ weakly in $L^2(\Omega;\mathbb{R}^{d\times d})$,*

where $\boldsymbol{u} \in H_0^1(\Omega;\mathbb{R}^d)$ solves the weak formulation (11). Moreover, if we assume strict monotonicity for $\boldsymbol{\sigma}$ (i.e., the inequality in (2e) is strict for $\boldsymbol{\tau} \neq \boldsymbol{\eta}$), it holds that

- *$\boldsymbol{G}_{{\rm s},h}^k \underline{\boldsymbol{u}}_h \to \boldsymbol{\nabla}_{\rm s}\boldsymbol{u}$ strongly in $L^2(\Omega;\mathbb{R}^{d\times d})$.*

Finally, if the solution to (11) is unique, convergence extends to the whole sequence.

Proof. See Section 7.2. □

Remark 11 (Existence of a solution to the continuous problem)*.* Notice that a side result of the existence of discrete solutions proved in Theorem 8 together with the convergence results of Theorem 10 is the existence of a solution to the weak formulation (11).

Remark 12 (Discrete Korn inequality)*.* In Proposition 19 we give a proof of the discrete Korn inequality (29) based on the results of [7], which require further assumptions on the mesh. While we have the feeling that these assumptions could probably be relaxed, we postpone this topic to a future work. Notice that inequality (29) is not required to prove the error estimate of Theorem 15.

In order to prove error estimates, we stipulate the following additional assumptions on the stress-strain function $\boldsymbol{\sigma}$.

Assumption 13 (Stress-strain relation II)**.** There exist real numbers $\sigma^*, \sigma_* \in (0, +\infty)$ such that, for a.e. $\boldsymbol{x} \in \Omega$, and all $\boldsymbol{\tau}, \boldsymbol{\eta} \in \mathbb{R}^{d\times d}_{\rm sym}$,

$$\|\boldsymbol{\sigma}(\boldsymbol{x},\boldsymbol{\tau}) - \boldsymbol{\sigma}(\boldsymbol{x},\boldsymbol{\eta})\|_{d\times d} \leqslant \sigma^* \|\boldsymbol{\tau} - \boldsymbol{\eta}\|_{d\times d}, \qquad \text{(Lipschitz continuity)} \tag{30a}$$

$$(\boldsymbol{\sigma}(\boldsymbol{x},\boldsymbol{\tau}) - \boldsymbol{\sigma}(\boldsymbol{x},\boldsymbol{\eta})) : (\boldsymbol{\tau} - \boldsymbol{\eta}) \geqslant \sigma_* \|\boldsymbol{\tau} - \boldsymbol{\eta}\|_{d\times d}^2. \qquad \text{(strong monotonicity)} \tag{30b}$$

Remark 14 (Lipschitz continuity and strong monotonocity)*.* It has been proved in [1, Lemma 4.1] that, under the assumptions (9), the stress-strain tensor function for the Hencky–Mises model is strongly monotone and Lipschitz-continuous, namely Assumption 13 holds. Also the isotropic damage model satisfies Assumption 13 if the damage function in (5) is, for instance, such that $D(|\boldsymbol{\tau}|) = 1-(1+|\boldsymbol{\tau}|)^{-\frac{1}{2}}$.

Theorem 15 (Error estimate)**.** *Let Assumptions 1 and 13 hold, and let $(\mathcal{T}_h)_{h\in\mathcal{H}}$ be a regular mesh sequence. Let $\boldsymbol{u}$ be the unique solution to (1). Let a polynomial degree $k \geqslant 1$ be fixed, and, for all $h \in \mathcal{H}$, let $\underline{\boldsymbol{u}}_h$ be the unique solution to (24) on the mesh $\mathcal{T}_h$. Then, under the additional regularity $\boldsymbol{u} \in H^{k+2}(\mathcal{T}_h;\mathbb{R}^d)$ and $\boldsymbol{\sigma}(\cdot,\boldsymbol{\nabla}_{\rm s}\boldsymbol{u}) \in H^{k+1}(\mathcal{T}_h;\mathbb{R}^{d\times d})$, it holds*

$$\|\boldsymbol{\nabla}_{\rm s}\boldsymbol{u} - \boldsymbol{G}_{{\rm s},h}^k \underline{\boldsymbol{u}}_h\| + s_h(\underline{\boldsymbol{u}}_h,\underline{\boldsymbol{u}}_h)^{1/2} \leqslant C h^{k+1} \left(\|\boldsymbol{u}\|_{H^{k+2}(\mathcal{T}_h;\mathbb{R}^d)} + \|\boldsymbol{\sigma}(\cdot,\boldsymbol{\nabla}_{\rm s}\boldsymbol{u})\|_{H^{k+1}(\mathcal{T}_h;\mathbb{R}^{d\times d})} \right), \tag{31}$$

where C is a positive constant depending only on Ω, k, the mesh regularity parameter ϱ, the real numbers $\overline{\sigma}$, $\underline{\sigma}$, σ^*, σ_* appearing in (2) and in (30), and an upper bound of $\|\boldsymbol{f}\|$.

Proof. See Section 7.3. □

5 Local principle of virtual work and law of action and reaction

We show in this section that the solution of the discrete problem (24) satisfies a local principle of virtual work with numerical tractions that obey the law of action and reaction. This property is important from both the mathematical and engineering points of view, and it can simplify the derivation of a posteriori error estimators based on equilibrated tractions.

Define, for all $T \in \mathcal{T}_h$, the space

$$\underline{\boldsymbol{D}}_{\partial T}^k := \bigtimes_{F \in \mathcal{F}_T} \mathbb{P}^k(F; \mathbb{R}^d),$$

as well as the boundary difference operator $\underline{\boldsymbol{\delta}}_{\partial T}^k : \underline{\boldsymbol{U}}_T^k \to \underline{\boldsymbol{D}}_{\partial T}^k$ such that, for all $\underline{\boldsymbol{v}}_T \in \underline{\boldsymbol{U}}_T^k$,

$$\underline{\boldsymbol{\delta}}_{\partial T}^k \underline{\boldsymbol{v}}_T = (\boldsymbol{\delta}_F^k \underline{\boldsymbol{v}}_T)_{F \in \mathcal{F}_T} := (\boldsymbol{v}_F - \boldsymbol{v}_T)_{F \in \mathcal{F}_T}.$$

The following proposition shows that the stabilization can be reformulated in terms of boundary differences.

Proposition 16 (Reformulation of the local stabilization bilinear form)**.** *For all mesh element $T \in \mathcal{T}_h$, the local stabilization bilinear form s_T defined by (26) satisfies, for all $\underline{\boldsymbol{u}}_T, \underline{\boldsymbol{v}}_T \in \underline{\boldsymbol{U}}_T^k$,*

$$s_T(\underline{\boldsymbol{u}}_T, \underline{\boldsymbol{v}}_T) = \tilde{s}_T(\underline{\boldsymbol{\delta}}_{\partial T}^k \underline{\boldsymbol{u}}_T, \underline{\boldsymbol{\delta}}_{\partial T}^k \underline{\boldsymbol{v}}_T),$$

with bilinear form $\tilde{s}_T : \underline{\boldsymbol{D}}_{\partial T}^k \times \underline{\boldsymbol{D}}_{\partial T}^k \to \mathbb{R}$ such that, for all $\underline{\boldsymbol{\alpha}}_{\partial T}, \underline{\boldsymbol{\beta}}_{\partial T} \in \underline{\boldsymbol{D}}_{\partial T}^k$,

$$\tilde{s}_T(\underline{\boldsymbol{\alpha}}_{\partial T}, \underline{\boldsymbol{\beta}}_{\partial T}) := s_T((\boldsymbol{0}, \underline{\boldsymbol{\alpha}}_{\partial T}), (\boldsymbol{0}, \underline{\boldsymbol{\beta}}_{\partial T})). \tag{32}$$

Proof. Let a mesh element $T \in \mathcal{T}_h$ be fixed. Using the fact that $\boldsymbol{r}_T^{k+1} \underline{\boldsymbol{I}}_T^k \boldsymbol{v}_T = \boldsymbol{v}_T$ for all $\boldsymbol{v}_T \in \mathbb{P}^k(T)^d$ (this because $\boldsymbol{r}_T^{k+1} \underline{\boldsymbol{I}}_T^k$ is a projector on $\mathbb{P}^{k+1}(T; \mathbb{R}^d)$, cf. [17, Eq. (20)]) together with the linearity of $\boldsymbol{r}_T^{k+1}$, it is inferred that, for all $F \in \mathcal{F}_T$, the face-based residual defined by (27) satisfies

$$\boldsymbol{\Delta}_{TF}^k \underline{\boldsymbol{v}}_T = \boldsymbol{\pi}_F^k(\boldsymbol{r}_T^{k+1}(\boldsymbol{0}, \underline{\boldsymbol{\delta}}_{\partial T}^k \underline{\boldsymbol{v}}_T) - \boldsymbol{\delta}_F^k \underline{\boldsymbol{v}}_T) - \boldsymbol{\pi}_T^k \boldsymbol{r}_T^{k+1}(\boldsymbol{0}, \underline{\boldsymbol{\delta}}_{\partial T}^k \underline{\boldsymbol{v}}_T) = \boldsymbol{\Delta}_{TF}^k(\boldsymbol{0}, \underline{\boldsymbol{\delta}}_{\partial T}^k \underline{\boldsymbol{v}}_T)$$

for all $\underline{\boldsymbol{v}}_T \in \underline{\boldsymbol{U}}_T^k$. Plugging this expression into (26) yields the assertion. □

Define the boundary residual operator $\underline{\boldsymbol{R}}_{\partial T}^k : \underline{\boldsymbol{U}}_T^k \to \underline{\boldsymbol{D}}_{\partial T}^k$ such that, for all $\underline{\boldsymbol{v}}_T \in \underline{\boldsymbol{U}}_T^k$, $\underline{\boldsymbol{R}}_{\partial T}^k \underline{\boldsymbol{v}}_T := (\boldsymbol{R}_{TF}^k \underline{\boldsymbol{v}}_T)_{F \in \mathcal{F}_T}$ satisfies

$$-\sum_{F \in \mathcal{F}_T} \int_F \boldsymbol{R}_{TF}^k \underline{\boldsymbol{v}}_T \cdot \boldsymbol{\alpha}_F = \tilde{s}_T(\underline{\boldsymbol{\delta}}_{\partial T}^k \underline{\boldsymbol{v}}_T, \underline{\boldsymbol{\alpha}}_{\partial T}) \qquad \forall \underline{\boldsymbol{\alpha}}_{\partial T} \in \underline{\boldsymbol{D}}_{\partial T}^k. \tag{33}$$

Problem (33) is well-posed, and computing $\boldsymbol{R}_{TF}^k \underline{\boldsymbol{v}}_T$ requires to invert the boundary mass matrix.

Lemma 17 (Local principle of virtual work and law of action and reaction)**.** *Denote by $\underline{\boldsymbol{u}}_h \in \underline{\boldsymbol{U}}_{h,0}^k$ a solution of problem (24) and, for all $T \in \mathcal{T}_h$ and all $F \in \mathcal{F}_T$, define the numerical traction*

$$\boldsymbol{T}_{TF}(\underline{\boldsymbol{u}}_T) := -\boldsymbol{\pi}_T^k \boldsymbol{\sigma}(\cdot, \boldsymbol{G}_{\mathrm{s},T}^k \underline{\boldsymbol{u}}_T) \boldsymbol{n}_{TF} + \boldsymbol{R}_{TF}^k \underline{\boldsymbol{u}}_T.$$

Then, for all $T \in \mathcal{T}_h$ we have the following discrete principle of virtual work: For all $\boldsymbol{v}_T \in \mathbb{P}^k(T; \mathbb{R}^d)$,

$$\int_T \boldsymbol{\sigma}(\cdot, \boldsymbol{G}_{\mathrm{s},T}^k \underline{\boldsymbol{u}}_T) : \boldsymbol{\nabla}_{\mathrm{s}} \boldsymbol{v}_T + \sum_{F \in \mathcal{F}_T} \int_F \boldsymbol{T}_{TF}(\underline{\boldsymbol{u}}_T) \cdot \boldsymbol{v}_T = \int_T \boldsymbol{f} \cdot \boldsymbol{v}_T, \tag{34}$$

and, for any interface $F \in \mathcal{F}_{T_1} \cap \mathcal{F}_{T_2}$, the numerical tractions satisfy the law of action and reaction:

$$\boldsymbol{T}_{T_1 F}(\underline{\boldsymbol{u}}_{T_1}) + \boldsymbol{T}_{T_2 F}(\underline{\boldsymbol{u}}_{T_2}) = \boldsymbol{0}. \tag{35}$$

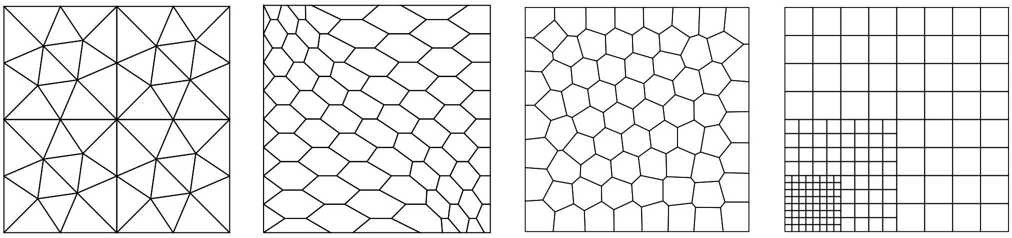

Figure 2: Triangular, hexagonal-dominant, Voronoi, and nonmatching quadrangular meshes for the numerical tests. The triangular and nonmatching quadrangular meshes were originally proposed for the FVCA5 benchmark [29]. The (predominantly) hexagonal was used in [18]. The Voronoi mesh family was obtained using the PolyMesher algorithm of [39].

Proof. For all $T \in \mathcal{T}_h$, use the definition (17) of $\boldsymbol{G}_{\mathrm{s},T}^k \underline{\boldsymbol{v}}_T$ with $\boldsymbol{\tau} = \boldsymbol{\pi}_T^k \boldsymbol{\sigma}(\cdot \boldsymbol{G}_{\mathrm{s},T}^k \underline{\boldsymbol{u}}_T)$ in A_h and the rewriting (32) of s_T together with the definition (33) of $\boldsymbol{R}_{TF}^k$ to infer that it holds, for all $\underline{\boldsymbol{v}}_h \in \underline{\boldsymbol{U}}_h^k$,

$$\int_\Omega \boldsymbol{f} \cdot \boldsymbol{v}_h = A_h(\underline{\boldsymbol{u}}_h, \underline{\boldsymbol{v}}_h) + s_h(\underline{\boldsymbol{u}}_h, \underline{\boldsymbol{v}}_h) =$$
$$\sum_{T \in \mathcal{T}_h} \left(\int_T \boldsymbol{\sigma}(\cdot, \boldsymbol{G}_{\mathrm{s},T}^k \underline{\boldsymbol{u}}_T) : \boldsymbol{\nabla}_{\mathrm{s}} \boldsymbol{v}_T + \sum_{F \in \mathcal{F}_T} \int_F (\boldsymbol{\pi}_T^k \boldsymbol{\sigma}(\cdot, \boldsymbol{G}_{\mathrm{s},T}^k \underline{\boldsymbol{u}}_T) \boldsymbol{n}_{TF} - \boldsymbol{R}_{TF}^k \underline{\boldsymbol{u}}_T) \cdot (\boldsymbol{v}_F - \boldsymbol{v}_T) \right),$$

where to cancel $\boldsymbol{\pi}_T^k$ inside the first integral in the second line we have used the fact that $\boldsymbol{\nabla}_{\mathrm{s}} \boldsymbol{v}_T \in \mathbb{P}^{k-1}(T; \mathbb{R}^{d \times d})$ for all $T \in \mathcal{T}_h$. Selecting $\underline{\boldsymbol{v}}_h$ such that $\boldsymbol{v}_T$ spans $\mathbb{P}^k(T; \mathbb{R}^d)$ for a selected mesh element $T \in \mathcal{T}_h$ while $\boldsymbol{v}_{T'} \equiv \boldsymbol{0}$ for all $T' \in \mathcal{T}_h \backslash \{T\}$ and $\boldsymbol{v}_F \equiv \boldsymbol{0}$ for all $F \in \mathcal{F}_h$, we obtain (34). On the other hand, selecting $\underline{\boldsymbol{v}}_h$ such that $\boldsymbol{v}_T \equiv \boldsymbol{0}$ for all $T \in \mathcal{T}_h$, $\boldsymbol{v}_F$ spans $\mathbb{P}^k(F; \mathbb{R}^d)$ for a selected interface $F \in \mathcal{F}_{T_1} \cap \mathcal{F}_{T_2}$, and $\boldsymbol{v}_{F'} \equiv \boldsymbol{0}$ for all $F' \in \mathcal{F}_h \backslash \{F\}$ yields (35). $\square$

6 Numerical results

In this section we present a comprehensive set of numerical tests to assess the properties of our method using the models of Examples 2, 3, and 5 (cf. also Remark 6).

6.1 Convergence for the Hencky–Mises model

In order to check the error estimates stated in Theorem 15, we first solve a manufactured two-dimensional hyperelasticity problem. We consider the Henky–Mises model with $\Phi(\rho) = \mu(e^{-\rho} + 2\rho)$ and $\alpha = \lambda + \mu$ in (8), so that conditions (9) are satisfied. This choice leads to the following stress-strain relation:

$$\boldsymbol{\sigma}(\boldsymbol{\nabla}_{\mathrm{s}} \boldsymbol{u}) = ((\lambda - \mu) + \mu e^{-\operatorname{dev}(\boldsymbol{\nabla}_{\mathrm{s}} \boldsymbol{u})}) \operatorname{tr}(\boldsymbol{\nabla}_{\mathrm{s}} \boldsymbol{u}) \boldsymbol{I}_d + \mu(2 - e^{-\operatorname{dev}(\boldsymbol{\nabla}_{\mathrm{s}} \boldsymbol{u})}) \boldsymbol{\nabla}_{\mathrm{s}} \boldsymbol{u}. \tag{36}$$

We consider the unit square domain $\Omega = (0,1)^2$ and take $\mu = 2$, $\lambda = 1$, and an exact displacement $\boldsymbol{u}$ given by

$$\boldsymbol{u}(\boldsymbol{x}) = \big(\sin(\pi x_1) \sin(\pi x_2), \sin(\pi x_1) \sin(\pi x_2) \big).$$

The volumetric load $\boldsymbol{f} = -\boldsymbol{\nabla} \cdot \boldsymbol{\sigma}(\boldsymbol{\nabla}_{\mathrm{s}} \boldsymbol{u})$ is inferred from the exact solution $\boldsymbol{u}$. In this case, since the selected exact displacement vanishes on Γ, we simply consider homogeneous Dirichlet conditions. We consider the triangular, hexagonal, Voronoi, and nonmatching quadrangular mesh families depicted in Figure 2 and polynomial degrees k ranging from 1 to 4. The nonmatching mesh is simply meant to show that the method supports nonconforming interfaces: refining in the corner has no particular meaning for the selected solution. Furthermore, the initialization of our iterative linearization procedure (Newton scheme) is obtained solving the linear elasticity model. This initial guess leads to a 40% reduction of the number of iterations with respect to a null initial guess. The energy-norm convergence rates displayed in the left column of Figure 3 are in agreement with the theoretical predictions. For the sake of completeness, we also display in the right column of Figure 3 the L^2-norm of the error defined as the difference between the L^2-projection $\boldsymbol{\pi}_h^k \boldsymbol{u}$ of the exact solution on $\mathbb{P}^k(\mathcal{T}_h; \mathbb{R}^d)$

and the broken polynomial function $\boldsymbol{u}_h$ obtained from element-based DOFs. In this case, orders of convergence up to h^{k+2} are observed.

6.2 Tensile and shear test cases

We next consider the two test cases schematically depicted in Figures 4 and 5. On the unit square domain Ω, we solve problem (1) considering three different models of hyperelasticity (see Remark 6):

(i) *Linear.* The linear model corresponding to the stored energy density function (7) with Lamé's parameters

$$\lambda = 11 \times 10^5\text{Pa},\ \ \mu = 82 \times 10^4\text{Pa}. \tag{37}$$

(ii) *Hencky–Mises.* The Hencky–Mises model (4) obtained by taking $\Phi(\rho) = \mu(\frac{\rho}{2} + (1+\rho)^{1/2})$ and $\alpha = \lambda + \mu$ in (8), with λ, μ as in (37) (also in this case conditions (9) hold). This choice leads to

$$\boldsymbol{\sigma}(\boldsymbol{\nabla}_{\rm s}\boldsymbol{u}) = ((\lambda + \frac{\mu}{2}) - \frac{\mu}{2}(1+\operatorname{dev}(\boldsymbol{\nabla}_{\rm s}\boldsymbol{u}))^{-1/2}) \operatorname{tr}(\boldsymbol{\nabla}_{\rm s}\boldsymbol{u})\boldsymbol{I}_d + \mu(1+(1+\operatorname{dev}(\boldsymbol{\nabla}_{\rm s}\boldsymbol{u}))^{-1/2})\boldsymbol{\nabla}_{\rm s}\boldsymbol{u}. \tag{38}$$

The Lamé's functions of the previous relation are inspired from those proposed in [4, Section 5.1]. In particular, the function $\tilde{\mu}(\rho) = \mu(1 + (1 + \operatorname{dev}(\boldsymbol{\nabla}_{\rm s}\boldsymbol{u}))^{-1/2})$ corresponds to the Carreau law for viscoplastic materials.

(iii) *Second-order.* The second-order model (6) with Lamé's parameter as in (37) and second-order moduli

$$A = 11 \times 10^6\text{Pa},\ \ \mathrm{B} = -48 \times 10^5\text{Pa},\ \ \mathrm{C} = 13.2 \times 10^5\text{Pa}.$$

These values correspond to the estimates provided in [30] for the Armco Iron. We recall that the second-order elasticity stress-strain relation does not satisfy in general the assumptions under which we are able to prove the convergence and error estimates. In particular, we observe that the stored energy density function defined in (10) is not convex.

The bottom part of the boundary of the domain is assumed to be fixed, the normal stress is equal to zero on the two lateral parts, and a traction is imposed at the top of the boundary. So, mixed boundary conditions are imposed as follows

$$\boldsymbol{u} = \boldsymbol{0} \quad \text{on } \{\boldsymbol{x} \in \Gamma, x_2 = 0\}, \tag{39a}$$
$$\boldsymbol{\sigma n} = \boldsymbol{T} \ \text{on } \{\boldsymbol{x} \in \Gamma, x_2 = 1\}, \tag{39b}$$
$$\boldsymbol{\sigma n} = \boldsymbol{0} \ \text{on } \{\boldsymbol{x} \in \Gamma, x_1 = 0\}, \tag{39c}$$
$$\boldsymbol{\sigma n} = \boldsymbol{0} \ \text{on } \{\boldsymbol{x} \in \Gamma, x_1 = 1\}. \tag{39d}$$

For the tensile case, we impose a vertical traction at the top of the boundary equal to $\boldsymbol{T} = (0, 3.2 \times 10^5\text{Pa})$. This type of boundary conditions produces large normal stresses (i.e., the diagonal components of $\boldsymbol{\sigma}$) and minor shear stresses (i.e., the off-diagonal components of $\boldsymbol{\sigma}$). It can be observed in Figure 4, where the components of the stress tensor are depicted for the linear case. In Figure 6 we plot the stress norm on the deformed domain obtained for the three hyperelasticity models. The results of Fig. 4, 5, 6, and 7 are obtained on a mesh with 3584 triangles (corresponding to a typical mesh-size of 3.84×10^{-3}) and with polynomial degree $k = 2$. Obviously, the symmetry of the results is visible, and we observe that the three displacement fields are very close. This is motivated by the fact that, with our choice of the parameters in (37) and in (38), the linear model exactly corresponds to the linear approximation at the origin of the nonlinear ones. The maximum value of the stress concentrates on the two bottom corners due to the homogeneous Dirichlet condition that totally locks the displacement when $x_1 = 0$. The repartition of the stress on the domain with the second-order model is visibly different from those obtained with the linear and Hencky–Mises models. At the energy level, we also have a higher difference between the second-order model and the linear one since $|\mathbb{E}_{\rm lin} - \mathbb{E}_{\rm hm}|/\mathbb{E}_{\rm lin} = 0.44\%$ while $|\mathbb{E}_{\rm lin} - \mathbb{E}_{\rm snd}|/\mathbb{E}_{\rm lin} = 4.45\%$, where $\mathbb{E}_\bullet$ is the total elastic energy obtained by integrating over the domain the strain energy density functions defined by (7), (8), and (10):

$$\mathbb{E}_\bullet := \int_\Omega \Psi_\bullet, \quad \text{with} \quad \bullet \in \{\text{lin}, \text{hm}, \text{snd}\}.$$

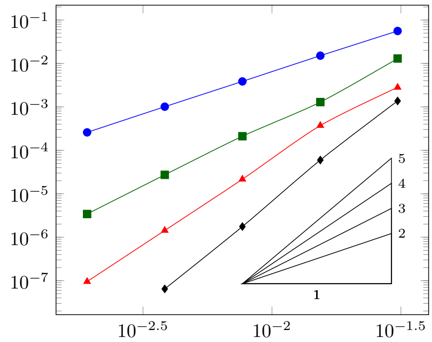

(a) Triangular, $\|\boldsymbol{\nabla}_{\rm s}\boldsymbol{u} - \boldsymbol{G}_{{\rm s},h}^k \underline{\boldsymbol{u}}_h\|$ vs. h

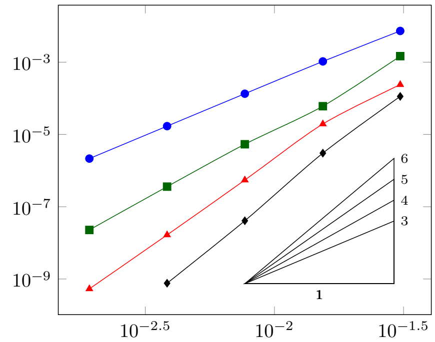

(b) Triangular, $\|\boldsymbol{\pi}_h^k \boldsymbol{u} - \boldsymbol{u}_h\|$ vs. h

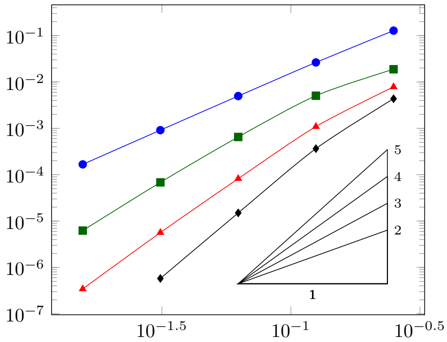

(c) Nonmatching, $\|\boldsymbol{\nabla}_{\rm s}\boldsymbol{u} - \boldsymbol{G}_{{\rm s},h}^k \underline{\boldsymbol{u}}_h\|$ vs. h

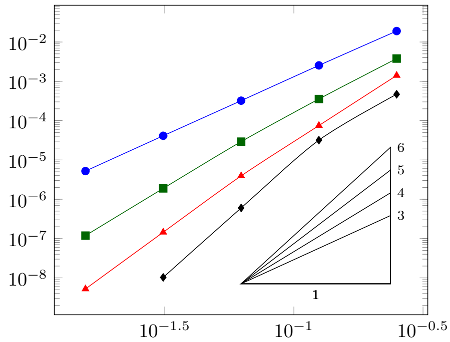

(d) Nonmatching, $\|\boldsymbol{\pi}_h^k \boldsymbol{u} - \boldsymbol{u}_h\|$ vs. h

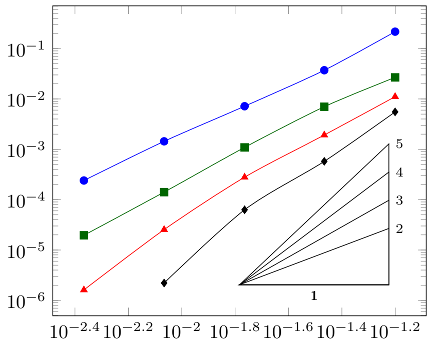

(e) Hexagonal, $\|\boldsymbol{\nabla}_{\rm s}\boldsymbol{u} - \boldsymbol{G}_{{\rm s},h}^k \underline{\boldsymbol{u}}_h\|$ vs. h

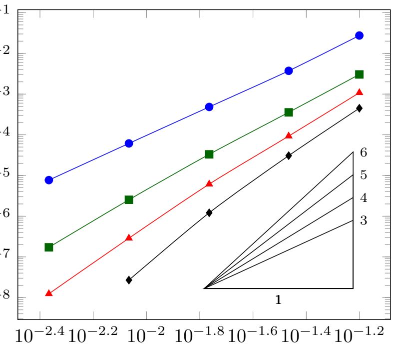

(f) Hexagonal, $\|\boldsymbol{\pi}_h^k \boldsymbol{u} - \boldsymbol{u}_h\|$ vs. h

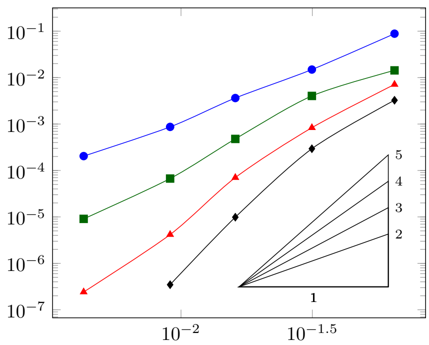

(g) Voronoi, $\|\boldsymbol{\nabla}_{\rm s}\boldsymbol{u} - \boldsymbol{G}_{{\rm s},h}^k \underline{\boldsymbol{u}}_h\|$ vs. h

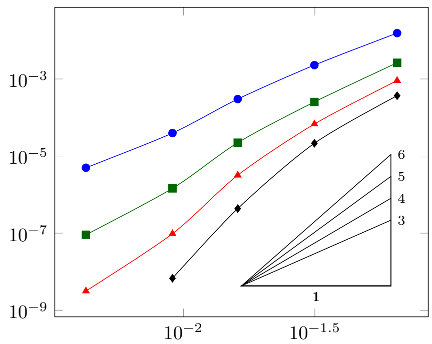

(h) Voronoi, $\|\boldsymbol{\pi}_h^k \boldsymbol{u} - \boldsymbol{u}_h\|$ vs. h

Figure 3: Convergence rates for polynomial degree k from 1 to 4 and mesh families of Figure 2.

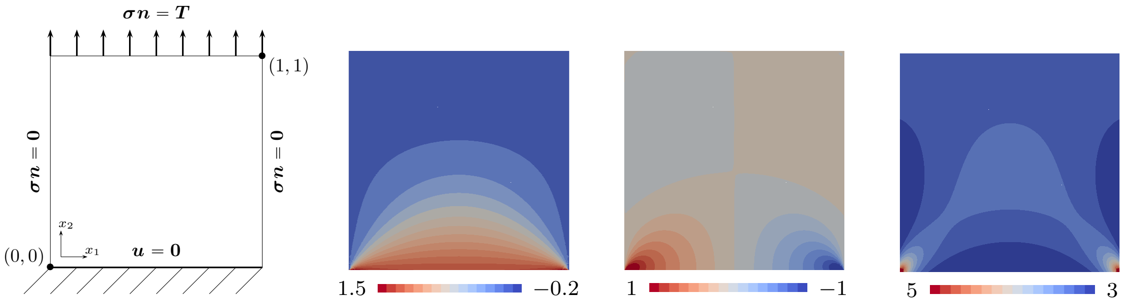

(a) Description (b) $\sigma_{1,1}$ (c) $\sigma_{1,2}$ (d) $\sigma_{2,2}$

Figure 4: Tensile test description and resulting stress components for the linear case. Values in 10^5Pa

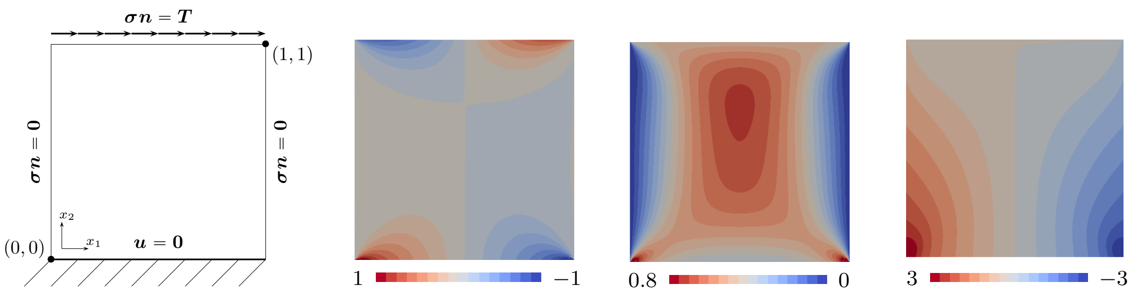

(a) Description (b) $\sigma_{1,1}$ (c) $\sigma_{1,2}$ (d) $\sigma_{2,2}$

Figure 5: Shear test description and resulting stress components for the linear case. Values in 10^5Pa

The reference values for the total energy, used in Figure 8 in order to assess convergence, are obtained on a fine Cartesian mesh having a mesh-size of 1.95×10^{-3} and $k = 3$.

For the shear case, we consider an horizontal traction equal to $\boldsymbol{T} = (4.5 \times 10^4\text{Pa}, 0)$ which induces the stress pattern illustrated in Figure 5. The computed stress norm on the deformed domain is depicted in Figure 7, and we can see that the displacement fields associated with the three models are very close as for the tensile test case. Here, the maximum values of the stress are localized in the lower part of the domain near the lateral parts. Unlike the tensile test, the difference between the three models is tiny as confirmed by the elastic energy equal to 3180 J, 3184 J, and 3190 J respectively. The decreasing of the energy difference in comparison with the previous test can be explained by the fact that the value of the Neumann boundary data on the top is divided by a factor 7 in order to obtain maximum displacements roughly equal to 15%.

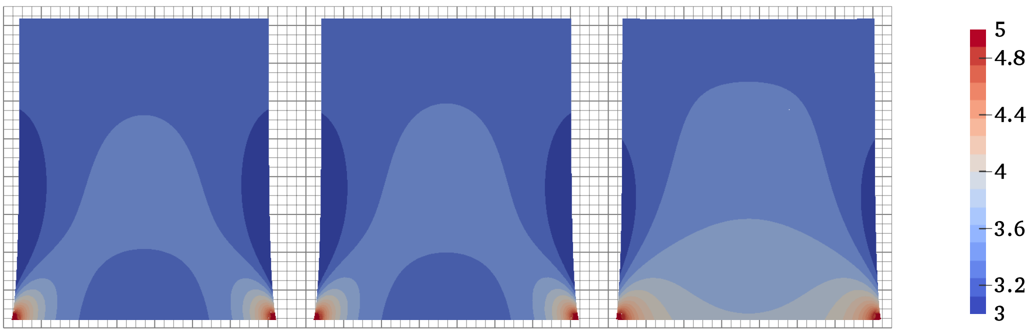

(a) Linear (b) Hencky–Mises (c) Second order

Figure 6: Tensile test case: Stress norm on the deformed domain. Values in 10^5Pa

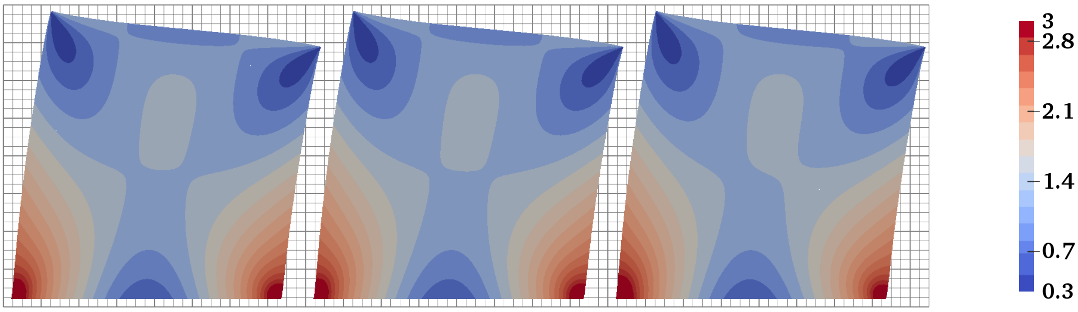

(a) Linear (b) Hencky–Mises (c) Second order

Figure 7: Shear test case: Stress norm on the deformed domain. Values in 10^5Pa

7 Analysis

We collect here the proofs of the results stated in Section 4.4. To alleviate the notation, from this point on we abridge into $a \lesssim b$ the inequality $a \leqslant Cb$ with real number $C > 0$ independent of h.

7.1 Existence and uniqueness

Proof of Theorem 8. 1) *Existence.* We follow the argument of [11, Theorem 3.3]. If $(E, (\cdot,\cdot)_E, \|\cdot\|_E)$ is a Euclidean space and $\Phi : E \to E$ is a continuous map such that $\frac{(\Phi(x),x)_E}{\|x\|_E} \to +\infty$, as $\|x\|_E \to +\infty$, then Φ is surjective. We take $E = \underline{\boldsymbol{U}}_{h,0}^k$, endowed with the inner product

$$(\underline{\boldsymbol{v}}_T, \underline{\boldsymbol{w}}_T)_{\epsilon,h} := \sum_{T\in\mathcal{T}_h} \left(\int_T \boldsymbol{\nabla}_{\mathrm{s}} \boldsymbol{v}_T : \boldsymbol{\nabla}_{\mathrm{s}} \boldsymbol{w}_T + \sum_{F\in\mathcal{F}_T} \frac{1}{h_F} \int_F (\boldsymbol{v}_F - \boldsymbol{v}_T) \cdot (\boldsymbol{w}_F - \boldsymbol{w}_T) \right),$$

and we define $\Phi : \underline{\boldsymbol{U}}_{h,0}^k \to \underline{\boldsymbol{U}}_{h,0}^k$ such that, for all $\underline{\boldsymbol{v}}_h \in \underline{\boldsymbol{U}}_{h,0}^k$, $(\Phi(\underline{\boldsymbol{v}}_h), \underline{\boldsymbol{w}}_h)_{\epsilon,h} = a_h(\underline{\boldsymbol{v}}_h, \underline{\boldsymbol{w}}_h)$ for all $\underline{\boldsymbol{w}}_h \in \underline{\boldsymbol{U}}_{h,0}^k$. The coercivity (2d) of $\boldsymbol{\sigma}$ together with the norm equivalence (28) yields $(\Phi(\underline{\boldsymbol{v}}_h), \underline{\boldsymbol{v}}_h)_{\epsilon,h} \geqslant \min\{1, \underline{\sigma}\}\eta^{-1}\|\underline{\boldsymbol{v}}_h\|_{\epsilon,h}^2$ for all $\underline{\boldsymbol{v}}_h \in \underline{\boldsymbol{U}}_{h,0}^k$, so that Φ is surjective. Let now $\underline{\boldsymbol{y}}_h \in \underline{\boldsymbol{U}}_{h,0}^k$ be such that $(\underline{\boldsymbol{y}}_h, \underline{\boldsymbol{w}}_h)_{\epsilon,h} = \int_\Omega \boldsymbol{f} \cdot \boldsymbol{w}_h$ for all $\underline{\boldsymbol{w}}_h \in \underline{\boldsymbol{U}}_{h,0}^k$. By the surjectivity of Φ, there exists $\underline{\boldsymbol{u}}_h \in \underline{\boldsymbol{U}}_{h,0}^k$ such that $\Phi(\underline{\boldsymbol{u}}_h) = \underline{\boldsymbol{y}}_h$. By definition of Φ and $\underline{\boldsymbol{y}}_h$, $\underline{\boldsymbol{u}}_h$ is a solution to the problem (24).

2) *Uniqueness.* Let $\underline{\boldsymbol{u}}_{h,1}, \underline{\boldsymbol{u}}_{h,2} \in \underline{\boldsymbol{U}}_{h,0}^k$ solve (24). We assume $\underline{\boldsymbol{u}}_{h,1} \neq \underline{\boldsymbol{u}}_{h,2}$ and proceed by contradiction. Subtracting (24) for $\underline{\boldsymbol{u}}_{h,2}$ from (24) for $\underline{\boldsymbol{u}}_{h,1}$, it is inferred that $a_h(\underline{\boldsymbol{u}}_{h,1}, \underline{\boldsymbol{v}}_h) - a(\underline{\boldsymbol{u}}_{h,2}, \underline{\boldsymbol{v}}_h) = 0$ for all $\underline{\boldsymbol{v}}_h \in \underline{\boldsymbol{U}}_{h,0}^k$. Hence in particular, taking $\underline{\boldsymbol{v}}_h = \underline{\boldsymbol{u}}_{h,1} - \underline{\boldsymbol{u}}_{h,2}$ we obtain that

$$a_h(\underline{\boldsymbol{u}}_{h,1}, \underline{\boldsymbol{u}}_{h,1} - \underline{\boldsymbol{u}}_{h,2}) - a_h(\underline{\boldsymbol{u}}_{h,2}, \underline{\boldsymbol{u}}_{h,1} - \underline{\boldsymbol{u}}_{h,2}) = 0$$

On the other hand, owing to the strict monotonicity of $\boldsymbol{\sigma}$ and to the fact that the bilinear form s_h is positive semidefinite, we have that

$$\begin{aligned} &a_h(\underline{\boldsymbol{u}}_{h,1}, \underline{\boldsymbol{u}}_{h,1} - \underline{\boldsymbol{u}}_{h,2}) - a_h(\underline{\boldsymbol{u}}_{h,2}, \underline{\boldsymbol{u}}_{h,1} - \underline{\boldsymbol{u}}_{h,2}) \\ &\quad = \int_\Omega \left(\boldsymbol{\sigma}(\cdot, \boldsymbol{G}_{\mathrm{s},h}^k \underline{\boldsymbol{u}}_{h,1}) - \boldsymbol{\sigma}(\cdot, \boldsymbol{G}_{\mathrm{s},h}^k \underline{\boldsymbol{u}}_{h,2})\right) : \boldsymbol{G}_{\mathrm{s},h}^k(\underline{\boldsymbol{u}}_{h,1} - \underline{\boldsymbol{u}}_{h,2}) + s_h(\underline{\boldsymbol{u}}_{h,1} - \underline{\boldsymbol{u}}_{h,2}, \underline{\boldsymbol{u}}_{h,1} - \underline{\boldsymbol{u}}_{h,2}) > 0. \end{aligned}$$

Hence, $\underline{\boldsymbol{u}}_{h,1} = \underline{\boldsymbol{u}}_{h,2}$ and the conclusion follows. □

7.2 Convergence

This section contains the proof of Theorem 10 preceeded by a discrete Rellich–Kondrachov Lemma (cf. [8, Theorem 9.16]).

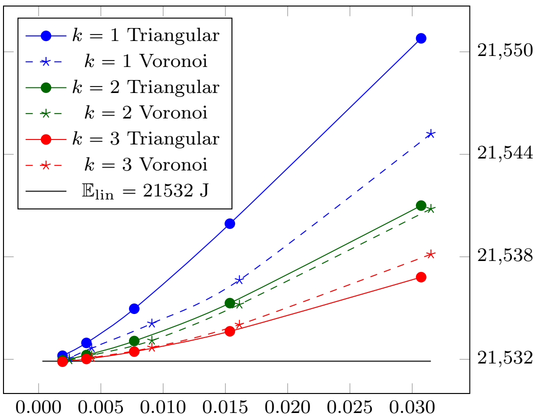

(a) Linear, tensile test

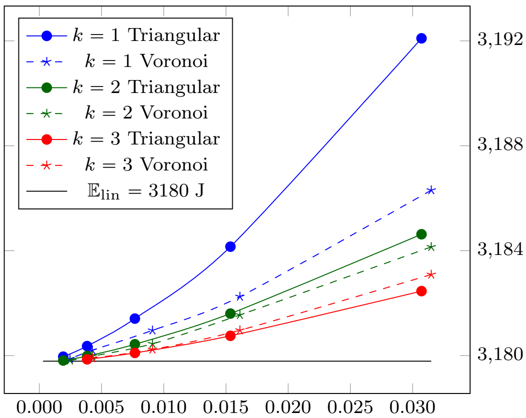

(b) Linear, shear test

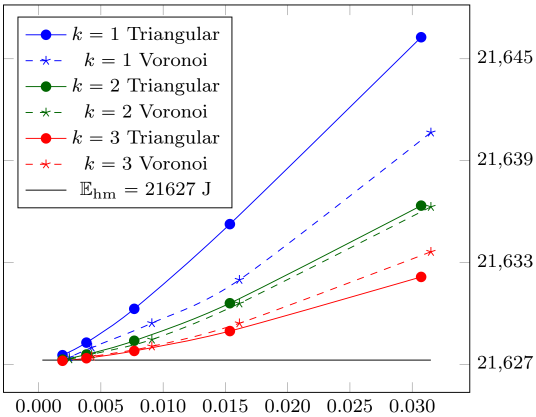

(c) Hencky–Mises, tensile test

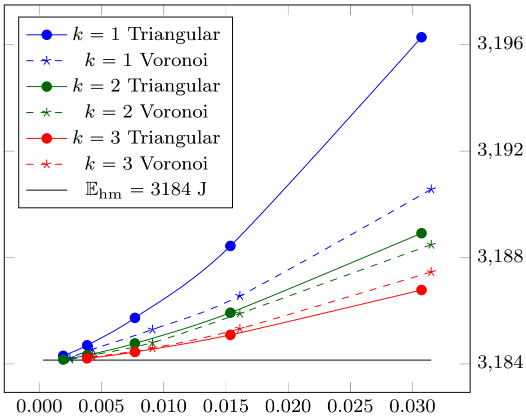

(d) Hencky–Mises, shear test

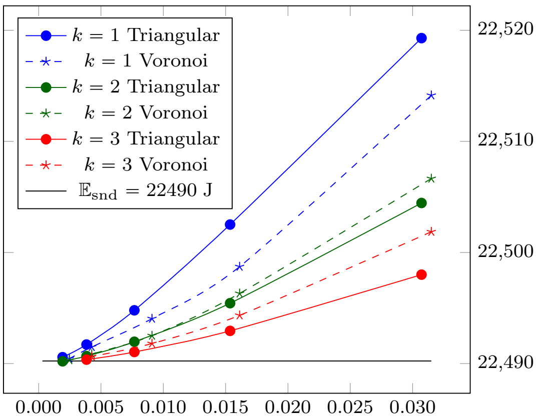

(e) Second-order, tensile test

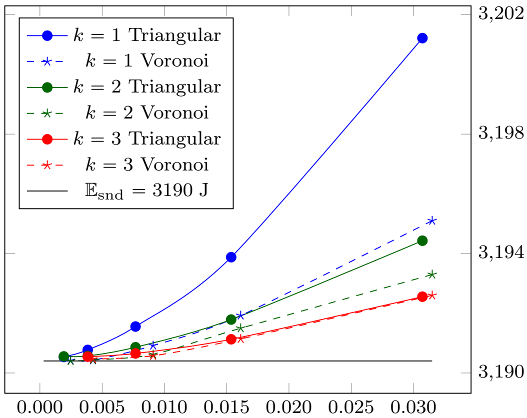

(f) Second-order, shear test

Figure 8: Energy vs h, tensile and shear test cases

Lemma 18 (Discrete compactness)**.** *Let the assumptions of Theorem 10 hold. Let* $(\underline{\boldsymbol{v}}_h)_{h\in\mathcal{H}} \in (\underline{\boldsymbol{U}}_{h,0}^k)_{h\in\mathcal{H}}$*, and assume that there is a real number* $C \geqslant 0$ *such that*

$$\|\underline{\boldsymbol{v}}_h\|_{\epsilon,h} \leqslant C \qquad \forall h \in \mathcal{H}. \tag{40}$$

Then, for all q *such that* $1 \leqslant q < +\infty$ *if* $d = 2$ *or* $1 \leqslant q < 6$ *if* $d = 3$*, the sequence* $(\boldsymbol{v}_h)_{h\in\mathcal{H}} \in (\mathbb{P}^k(\mathcal{T}_h;\mathbb{R}^d))_{h\in\mathcal{H}}$ *is relatively compact in* $L^q(\Omega;\mathbb{R}^d)$*. As a consequence, there is a function* $\boldsymbol{v} \in L^q(\Omega;\mathbb{R}^d)$ *such that as* $h \to 0$*, up to a subsequence,* $\boldsymbol{v}_h \to \boldsymbol{v}$ *strongly in* $L^q(\Omega;\mathbb{R}^d)$*.*

Proof. In the proof we use the same notation for functions in $L^2(\Omega;\mathbb{R}^d) \subset L^1(\Omega;\mathbb{R}^d)$ and for their extension by zero outside Ω. Let $(\underline{\boldsymbol{v}}_h)_{h\in\mathcal{H}} \in (\underline{\boldsymbol{U}}_{h,0}^k)_{h\in\mathcal{H}}$ be such that (40) holds. Define the space of integrable functions with bounded variation $\mathrm{BV}(\mathbb{R}^d) := \{\boldsymbol{v} \in L^1(\mathbb{R}^d;\mathbb{R}^d) \mid \|\boldsymbol{v}\|_{\mathrm{BV}} < +\infty\}$, where

$$\|\boldsymbol{v}\|_{\mathrm{BV}} := \sum_{i=1}^d \sup\left\{\int_{\mathbb{R}^d} \boldsymbol{v}\cdot\partial_i\boldsymbol{\phi} \;\middle|\; \boldsymbol{\phi} \in C_c^\infty(\mathbb{R}^d;\mathbb{R}^d), \|\boldsymbol{\phi}\|_{L^\infty(\mathbb{R}^d;\mathbb{R}^d)} \leqslant 1\right\}.$$

Here $\partial_i\boldsymbol{\phi}$ denotes the i-th column of $\boldsymbol{\nabla}\boldsymbol{\phi}$. Let $\boldsymbol{\phi} \in C_c^\infty(\mathbb{R}^d;\mathbb{R}^d)$ with $\|\boldsymbol{\phi}\|_{L^\infty(\mathbb{R}^d;\mathbb{R}^d)} \leqslant 1$. Integrating by parts and using the fact that $\sum_{T\in\mathcal{T}_h}\sum_{F\in\mathcal{F}_T}\int_F(\boldsymbol{v}_F\cdot\boldsymbol{\phi})\boldsymbol{n}_{TF} = 0$, we have that

$$\begin{aligned}
\int_{\mathbb{R}^d} \boldsymbol{v}_h\cdot\partial_i\boldsymbol{\phi} = \sum_{T\in\mathcal{T}_h}\int_T((\boldsymbol{\nabla}\boldsymbol{\phi})^{\mathrm{T}}\boldsymbol{v}_T)_i &= -\sum_{T\in\mathcal{T}_h}\left(\int_T((\boldsymbol{\nabla}\boldsymbol{v}_T)^{\mathrm{T}}\boldsymbol{\phi})_i + \sum_{F\in\mathcal{F}_T}\int_F(\boldsymbol{v}_F\cdot\boldsymbol{\phi} - \boldsymbol{v}_T\cdot\boldsymbol{\phi})(\boldsymbol{n}_{TF})_i\right)\\
&\leqslant \sum_{T\in\mathcal{T}_h}\left(\int_T\sum_{j=1}^d|(\boldsymbol{\nabla}\boldsymbol{v}_T)_{ji}| + \sum_{F\in\mathcal{F}_T}\int_F\sum_{j=1}^d|(\boldsymbol{v}_F - \boldsymbol{v}_T)_j(\boldsymbol{n}_{TF})_i|\right),
\end{aligned}$$

where, in order to pass to the second line, we have used $\|\boldsymbol{\phi}\|_{L^\infty(\mathbb{R}^d;\mathbb{R}^d)} \leqslant 1$. Therefore, summing over $i \in \{1,\ldots,d\}$, observing that, for all $T \in \mathcal{T}_h$ and all $F \in \mathcal{F}_T$, we have $\sum_{i=1}^d|(\boldsymbol{n}_{TF})_i| \leqslant d^{1/2}$, and using the Lebesgue embeddings arising from the Hölder inequality on bounded domain, leads to

$$\|\boldsymbol{v}_h\|_{\mathrm{BV}} \lesssim \sum_{T\in\mathcal{T}_h}\left(|T|_d^{1/2}\|\boldsymbol{\nabla}\boldsymbol{v}_T\|_T + \sum_{F\in\mathcal{F}_T}|F|_{d-1}^{1/2}\|\boldsymbol{v}_F - \boldsymbol{v}_T\|_F\right),$$

where $|\cdot|_d$ denotes the d-dimensional Hausdorff measure. Moreover, using the Cauchy–Schwarz inequality together with the geometric bound $|F|_{d-1}h_F \lesssim |T|_d$, we obtain that

$$\|\boldsymbol{v}_h\|_{\mathrm{BV}} \lesssim |\Omega|_d^{1/2}\left(\sum_{T\in\mathcal{T}_h}\left[\|\boldsymbol{\nabla}\boldsymbol{v}_T\|_T^2 + \sum_{F\in\mathcal{F}_T}h_F^{-1}\|\boldsymbol{v}_F - \boldsymbol{v}_T\|_F^2\right]\right)^{1/2}.$$

Thus, using the discrete Korn inequality (29), it is readily inferred that

$$\|\boldsymbol{v}_h\|_{\mathrm{BV}} \lesssim \|\underline{\boldsymbol{v}}_h\|_{\epsilon,h} \lesssim 1. \tag{41}$$

Owing to the Helly selection principle [25, Section 5.2.3], the sequence $(\boldsymbol{v}_h)_{h\in\mathcal{H}}$ is relatively compact in $L^1(\mathbb{R}^d;\mathbb{R}^d)$ and thus in $L^1(\Omega;\mathbb{R}^d)$. It only remains to prove that the sequence is also relatively compact in $L^q(\Omega;\mathbb{R}^d)$, with $1 < q < +\infty$ if $d = 2$ or $1 < q < 6$ if $d = 3$. Owing to the discrete Sobolev embeddings [15, Proposition 5.4] together with the discrete Korn inequality (29), it holds, with $r = q + 1$ if $d = 2$ and $r = 6$ if $d = 3$, that

$$\|\boldsymbol{v}_h\|_{L^r(\Omega;\mathbb{R}^d)} \lesssim \left(\sum_{T\in\mathcal{T}_h}\left[\|\boldsymbol{\nabla}\boldsymbol{v}_T\|_T^2 + \sum_{F\in\mathcal{F}_T}h_F^{-1}\|\boldsymbol{v}_F - \boldsymbol{v}_T\|_F^2\right]\right)^{1/2} \lesssim 1,$$

Thus, we can complete the proof by means of the interpolation inequality [8, Remark 2 p. 93]. For all $h, h' \in \mathcal{H}$ we have with $\theta := \frac{r-q}{q(r-1)} \in (0,1)$,

$$\|\boldsymbol{v}_h - \boldsymbol{v}_{h'}\|_{L^q(\Omega;\mathbb{R}^d)} \leqslant \|\boldsymbol{v}_h - \boldsymbol{v}_{h'}\|_{L^1(\Omega;\mathbb{R}^d)}^\theta\|\boldsymbol{v}_h - \boldsymbol{v}_{h'}\|_{L^r(\Omega;\mathbb{R}^d)}^{1-\theta} \lesssim \|\boldsymbol{v}_h - \boldsymbol{v}_{h'}\|_{L^1(\Omega;\mathbb{R}^d)}^\theta.$$

Therefore, up to a subsequence, $(\boldsymbol{v}_h)_{h\in\mathcal{H}}$ is a Cauchy sequence in $L^q(\Omega;\mathbb{R}^d)$, so it converges. $\square$

We are now ready to prove convergence.

Proof of Theorem 10. The proof is subdivided into four steps: in **Step 1** we prove a uniform a priori bound on the solutions of the discrete problem (24); in **Step 2** we infer the existence of a limit for the sequence of discrete solutions and investigate its regularity; in **Step 3** we show that this limit solves the continuous problem (11); finally, in **Step 4** we prove strong convergence.

Step 1: *A priori bound.* We start by showing the following uniform a priori bound on the sequence of discrete solutions:

$$\|\underline{\boldsymbol{u}}_h\|_{\epsilon,h} \leqslant C\|\boldsymbol{f}\|, \tag{42}$$

where the real number $C > 0$ only depends on $\Omega, \underline{\sigma}, \varrho$, and k. Making $\underline{\boldsymbol{v}}_h = \underline{\boldsymbol{u}}_h$ in (24) and using the coercivity property (2d) of $\boldsymbol{\sigma}$ in the left-hand side together with the Cauchy–Schwarz inequality in the right-hand side yields

$$\sum_{T\in\mathcal{T}_h}\left(\underline{\sigma}\|\boldsymbol{G}^k_{\mathrm{s},T}\underline{\boldsymbol{u}}_T\|_T^2 + \sum_{F\in\mathcal{F}_h} h_F^{-1}\|\boldsymbol{\Delta}^k_{TF}\underline{\boldsymbol{u}}_T\|_F^2\right) \leqslant \|\boldsymbol{f}\|\|\boldsymbol{u}_h\|.$$

Owing to the norm equivalence (28), and using the discrete Korn inequality (29) to estimate the right-hand side of the previous inequality, it is inferred that

$$\eta^{-1}\min(1,\underline{\sigma})\|\underline{\boldsymbol{u}}_h\|_{\epsilon,h}^2 \leqslant \|\boldsymbol{f}\|\|\boldsymbol{u}_h\| \leqslant C_{\mathrm{K}}\|\boldsymbol{f}\|\|\underline{\boldsymbol{u}}_h\|_{\epsilon,h}.$$

Dividing by $\|\underline{\boldsymbol{u}}_h\|_{\epsilon,h}$ yields (42) with $C = \eta\min(1,\underline{\sigma})^{-1}C_{\mathrm{K}}$.

Step 2: *Existence of a limit and regularity.* Let $1 \leqslant q < +\infty$ if $d = 2$ or $1 \leqslant q < 6$ if $d = 3$. Owing to the a priori bound (42) and the norm equivalence (28), the sequences $(\|\underline{\boldsymbol{u}}_h\|_{\epsilon,h})_{h\in\mathcal{H}}$ and $(\|\boldsymbol{G}^k_{\mathrm{s},h}\underline{\boldsymbol{u}}_h\|)_{h\in\mathcal{H}}$ are uniformly bounded. Therefore, Lemma 18 and the Kakutani theorem [8, Theorem 3.17] yield the existence of $\boldsymbol{u} \in L^q(\Omega;\mathbb{R}^d)$ and $\boldsymbol{\mathcal{G}} \in L^2(\Omega;\mathbb{R}^{d\times d})$ such that as $h \to 0$, up to a subsequence,

$$\boldsymbol{u}_h \to \boldsymbol{u} \text{ strongly in } L^q(\Omega;\mathbb{R}^d) \text{ and } \boldsymbol{G}^k_{\mathrm{s},h}\underline{\boldsymbol{u}}_h \to \boldsymbol{\mathcal{G}} \text{ weakly in } L^2(\Omega;\mathbb{R}^{d\times d}). \tag{43}$$

This together with the fact that $\boldsymbol{u}_{h,\Gamma} = \boldsymbol{0}$ on Γ, shows that, for any $\boldsymbol{\tau} \in H^1(\Omega;\mathbb{R}^{d\times d}_{\mathrm{sym}})$,

$$\begin{aligned}\left|\int_\Omega \boldsymbol{\mathcal{G}} : \boldsymbol{\tau} + \boldsymbol{u}\cdot(\boldsymbol{\nabla}\cdot\boldsymbol{\tau})\right| &= \lim_{h\to 0}\left|\int_\Omega \boldsymbol{G}^k_{\mathrm{s},h}\underline{\boldsymbol{u}}_h : \boldsymbol{\tau} + \boldsymbol{u}_h\cdot(\boldsymbol{\nabla}\cdot\boldsymbol{\tau}) - \int_\Gamma \boldsymbol{u}_{h,\Gamma}\cdot\boldsymbol{\gamma}_{\boldsymbol{n}}(\boldsymbol{\tau})\right| \\ &\leqslant \lim_{h\to 0}\left(\|\underline{\boldsymbol{u}}_h\|_{\epsilon,h}\max_{\underline{\boldsymbol{w}}_h\in\underline{\boldsymbol{U}}^k_h,\,\|\underline{\boldsymbol{w}}_h\|_{\epsilon,h}=1}\mathcal{R}_h(\underline{\boldsymbol{w}}_h,\boldsymbol{\tau})\right) = 0,\end{aligned} \tag{44}$$

with $\mathcal{R}_h$ defined by (21). To pass to the second line in (44) we have used the uniform bound (42) on $\|\underline{\boldsymbol{u}}_h\|_{\epsilon,h}$ and the sequential consistency (22) of $\boldsymbol{G}^k_{\mathrm{s},h}$. Applying the previous relation with $\boldsymbol{\tau} \in C^\infty_c(\Omega;\mathbb{R}^{d\times d}_{\mathrm{sym}})$ leads to $\int_\Omega \boldsymbol{\mathcal{G}} : \boldsymbol{\tau} + \boldsymbol{u}\cdot(\boldsymbol{\nabla}\cdot\boldsymbol{\tau}) = 0$, thus $\boldsymbol{\mathcal{G}} = \boldsymbol{\nabla}_{\mathrm{s}}\boldsymbol{u}$ in the sense of distributions on Ω. As a result, owing to the isomorphism of Hilbert spaces between $H^1(\Omega;\mathbb{R}^d)$ and $\{\boldsymbol{v} \in L^2(\Omega;\mathbb{R}^d) \mid \boldsymbol{\nabla}_{\mathrm{s}}\boldsymbol{v} \in L^2(\Omega;\mathbb{R}^{d\times d}_{\mathrm{sym}})\}$ proved in [24, Theorem 3.1], we infer that $\boldsymbol{u} \in H^1(\Omega;\mathbb{R}^d)$. Using again (44) with $\boldsymbol{\tau} \in H^1(\Omega;\mathbb{R}^{d\times d}_{\mathrm{sym}})$ and integrating by parts, we obtain $\int_\Gamma \boldsymbol{\gamma}(\boldsymbol{u})\cdot\boldsymbol{\gamma}_{\boldsymbol{n}}(\boldsymbol{\tau}) = 0$ with $\boldsymbol{\gamma}(\boldsymbol{u})$ denoting the trace of $\boldsymbol{u}$. As the set $\{\boldsymbol{\gamma}_{\boldsymbol{n}}(\boldsymbol{\tau})_{|\Gamma} : \boldsymbol{\tau} \in H^1(\Omega;\mathbb{R}^{d\times d}_{\mathrm{sym}})\}$ is dense in $L^2(\Gamma;\mathbb{R}^d)$, we deduce that $\boldsymbol{\gamma}(\boldsymbol{u}) = \boldsymbol{0}$ on Γ. In conclusion, with convergences up to a subsequence,

$$\boldsymbol{u} \in H^1_0(\Omega;\mathbb{R}^d),\ \boldsymbol{u}_h \to \boldsymbol{u} \text{ strongly in } L^q(\Omega;\mathbb{R}^d), \text{ and } \boldsymbol{G}^k_{\mathrm{s},h}\underline{\boldsymbol{u}}_h \to \boldsymbol{\nabla}_{\mathrm{s}}\boldsymbol{u} \text{ weakly in } L^2(\Omega;\mathbb{R}^{d\times d}).$$

Step 3: *Identification of the limit.* Let us now prove that $\boldsymbol{u}$ is a solution to (11). The growth property (2c) on $\boldsymbol{\sigma}$ and the bound on $(\|\boldsymbol{G}^k_{\mathrm{s},h}\underline{\boldsymbol{u}}_h\|)_{h\in\mathcal{H}}$ ensure that the sequence $(\boldsymbol{\sigma}(\cdot,\boldsymbol{G}^k_{\mathrm{s},h}\underline{\boldsymbol{u}}_h))_{h\in\mathcal{H}}$ is bounded in $L^2(\Omega;\mathbb{R}^{d\times d}_{\mathrm{sym}})$. Hence, there exists $\boldsymbol{\eta} \in L^2(\Omega;\mathbb{R}^{d\times d}_{\mathrm{sym}})$ such that, up to a subsequence as $h \to 0$,

$$\boldsymbol{\sigma}(\cdot,\boldsymbol{G}^k_{\mathrm{s},h}\underline{\boldsymbol{u}}_h) \to \boldsymbol{\eta} \quad \text{weakly in } L^2(\Omega;\mathbb{R}^{d\times d}). \tag{45}$$

Plugging into (24) $\underline{\boldsymbol{v}}_h = \underline{\boldsymbol{I}}_h^k \boldsymbol{\phi}$, with $\boldsymbol{\phi} \in C_c^\infty(\Omega; \mathbb{R}^d)$, gives

$$\int_\Omega \boldsymbol{\sigma}(\cdot, \boldsymbol{G}_{\mathrm{s},h}^k \underline{\boldsymbol{u}}_h) : \boldsymbol{G}_{\mathrm{s},h}^k \underline{\boldsymbol{I}}_h^k \boldsymbol{\phi} = \int_\Omega \boldsymbol{f} \cdot \boldsymbol{\pi}_h^k \boldsymbol{\phi} - s_h(\underline{\boldsymbol{u}}_h, \underline{\boldsymbol{I}}_h^k \boldsymbol{\phi}), \tag{46}$$

with $\boldsymbol{\pi}_h^k$ denoting the L^2-projector on the broken polynomial spaces $\mathbb{P}^k(\mathcal{T}_h; \mathbb{R}^d)$ and s_h defined by (26). Using the Cauchy–Schwarz inequality followed by the norm equivalence (28) to bound the first factor, we infer

$$|s_h(\underline{\boldsymbol{u}}_h, \underline{\boldsymbol{I}}_h^k \boldsymbol{\phi})| \leqslant s_h(\underline{\boldsymbol{u}}_h, \underline{\boldsymbol{u}}_h)^{1/2} s_h(\underline{\boldsymbol{I}}_h^k \boldsymbol{\phi}, \underline{\boldsymbol{I}}_h^k \boldsymbol{\phi})^{1/2} \lesssim \|\underline{\boldsymbol{u}}_h\|_{\epsilon,h} s_h(\underline{\boldsymbol{I}}_h^k \boldsymbol{\phi}, \underline{\boldsymbol{I}}_h^k \boldsymbol{\phi})^{1/2}. \tag{47}$$

It was proved in [17, Eq. (35)] using the optimal approximation properties of $\boldsymbol{r}_T^{k+1} \underline{\boldsymbol{I}}_T^k$ that it holds for all $h \in \mathcal{H}$, all $T \in \mathcal{T}_h$, all $\boldsymbol{v} \in H^{k+2}(T; \mathbb{R}^d)$, and all $F \in \mathcal{F}_T$ that

$$h_F^{-1/2} \|\boldsymbol{\Delta}_{TF}^k \underline{\boldsymbol{I}}_T^k \boldsymbol{v}\|_F \lesssim h_T^{k+1} \|\boldsymbol{v}\|_{H^{k+2}(T;\mathbb{R}^d)}, \tag{48}$$

with $\boldsymbol{\Delta}_{TF}^k$ defined by (27). As a consequence, recalling the definition (26) of s_h, we have the following convergence result:

$$\forall \boldsymbol{v} \in H^1(\Omega; \mathbb{R}^d) \cap H^2(\mathcal{T}_h; \mathbb{R}^d), \quad \lim_{h \to 0} s_h(\underline{\boldsymbol{I}}_h^k \boldsymbol{v}, \underline{\boldsymbol{I}}_h^k \boldsymbol{v}) = 0. \tag{49}$$

Recalling the a priori bound (42) on the discrete solution and the convergence property (49), it follows from (47) that $|s_h(\underline{\boldsymbol{u}}_h, \underline{\boldsymbol{I}}_h^k \boldsymbol{\phi})| \to 0$ as $h \to 0$. Additionally, by the approximation property (13a) of the L^2-projector, one has $\boldsymbol{\pi}_h^k \boldsymbol{\phi} \to \boldsymbol{\phi}$ strongly in $L^2(\Omega; \mathbb{R}^d)$ and, by virtue of Proposition 7, that $\boldsymbol{G}_{\mathrm{s},h}^k \underline{\boldsymbol{I}}_h^k \boldsymbol{\phi} \to \boldsymbol{\nabla}_{\mathrm{s}} \boldsymbol{\phi}$ strongly in $L^2(\Omega; \mathbb{R}^{d \times d})$. Thus, we can pass to the limit $h \to 0$ in (46) and obtain

$$\int_\Omega \boldsymbol{\eta} : \boldsymbol{\nabla}_{\mathrm{s}} \boldsymbol{\phi} = \int_\Omega \boldsymbol{f} \cdot \boldsymbol{\phi}. \tag{50}$$

By density of $C_c^\infty(\Omega; \mathbb{R}^d)$ in $H_0^1(\Omega; \mathbb{R}^d)$, this relation still holds if $\boldsymbol{\phi} \in H_0^1(\Omega; \mathbb{R}^d)$. On the other hand, plugging $\underline{\boldsymbol{v}}_h = \underline{\boldsymbol{u}}_h$ into (24) and using the fact that $s_h(\underline{\boldsymbol{u}}_h, \underline{\boldsymbol{u}}_h) \geqslant 0$, we obtain

$$\mathfrak{T}_h := \int_\Omega \boldsymbol{\sigma}(\cdot, \boldsymbol{G}_{\mathrm{s},h}^k \underline{\boldsymbol{u}}_h) : \boldsymbol{G}_{\mathrm{s},h}^k \underline{\boldsymbol{u}}_h \leqslant \int_\Omega \boldsymbol{f} \cdot \boldsymbol{u}_h.$$

Thus, using the previous bound, the strong convergence $\boldsymbol{u}_h \to \boldsymbol{u}$, and (50), it is inferred that

$$\lim_{h \to 0} \mathfrak{T}_h \leqslant \int_\Omega \boldsymbol{f} \cdot \boldsymbol{u} = \int_\Omega \boldsymbol{\eta} : \boldsymbol{\nabla}_{\mathrm{s}} \boldsymbol{u}. \tag{51}$$

We now use the monotonicity assumption on $\boldsymbol{\sigma}$ and the Minty trick [33] to prove that $\boldsymbol{\eta} = \boldsymbol{\sigma}(\cdot, \boldsymbol{\nabla}_{\mathrm{s}} \boldsymbol{u})$. Let $\boldsymbol{\Lambda} \in L^2(\Omega; \mathbb{R}^{d \times d})$ and write, using the monotonicity (2e) of $\boldsymbol{\sigma}$, the convergence (45) of $\boldsymbol{\sigma}(\cdot, \boldsymbol{G}_{\mathrm{s},h}^k \underline{\boldsymbol{u}}_h)$, and the bound (51),

$$0 \leqslant \lim_{h \to 0} \left(\int_\Omega (\boldsymbol{\sigma}(\cdot, \boldsymbol{G}_{\mathrm{s},h}^k \underline{\boldsymbol{u}}_h) - \boldsymbol{\sigma}(\cdot, \boldsymbol{\Lambda})) : (\boldsymbol{G}_{\mathrm{s},h}^k \underline{\boldsymbol{u}}_h - \boldsymbol{\Lambda}) \right) \leqslant \int_\Omega (\boldsymbol{\eta} - \boldsymbol{\sigma}(\cdot, \boldsymbol{\Lambda})) : (\boldsymbol{\nabla}_{\mathrm{s}} \boldsymbol{u} - \boldsymbol{\Lambda}). \tag{52}$$

Applying the previous relation with $\boldsymbol{\Lambda} = \boldsymbol{\nabla}_{\mathrm{s}} \boldsymbol{u} \pm t \boldsymbol{\nabla}_{\mathrm{s}} \boldsymbol{v}$, for $t > 0$ and $\boldsymbol{v} \in H_0^1(\Omega; \mathbb{R}^d)$, and dividing by t, leads to

$$0 \leqslant \pm \int_\Omega (\boldsymbol{\eta} - \boldsymbol{\sigma}(\cdot, \boldsymbol{\nabla}_{\mathrm{s}} \boldsymbol{u} \mp t \boldsymbol{\nabla}_{\mathrm{s}} \boldsymbol{v})) : \boldsymbol{\nabla}_{\mathrm{s}} \boldsymbol{v}.$$

Owing to the growth property (2c) and the Caratheodory property (2a) of $\boldsymbol{\sigma}$, we can let $t \to 0$ and pass the limit inside the integral and then inside the argument of $\boldsymbol{\sigma}$. In conclusion, for all $\boldsymbol{v} \in H_0^1(\Omega; \mathbb{R}^d)$, we infer

$$\int_\Omega \boldsymbol{\sigma}(\cdot, \boldsymbol{\nabla}_{\mathrm{s}} \boldsymbol{u}) : \boldsymbol{\nabla}_{\mathrm{s}} \boldsymbol{v} = \int_\Omega \boldsymbol{\eta} : \boldsymbol{\nabla}_{\mathrm{s}} \boldsymbol{v} = \int_\Omega \boldsymbol{f} \cdot \boldsymbol{v},$$

where we have used (50) with $\boldsymbol{\phi} = \boldsymbol{v}$ in order to obtain the second equality. The above equation shows that $\boldsymbol{\eta} = \boldsymbol{\sigma}(\cdot, \boldsymbol{\nabla}_{\mathrm{s}} \boldsymbol{u})$ and that $\boldsymbol{u}$ solves (11).

Step 4: ***Strong convergence.*** We prove that if $\boldsymbol{\sigma}$ is strictly monotone then $\boldsymbol{G}_{\mathrm{s},h}^k \underline{\boldsymbol{u}}_h \to \boldsymbol{\nabla}_{\mathrm{s}} \boldsymbol{u}$ strongly in $L^2(\Omega; \mathbb{R}^{d\times d})$. We define the function $\mathcal{D}_h : \Omega \to \mathbb{R}$ such that

$$\mathcal{D}_h := (\boldsymbol{\sigma}(\cdot, \boldsymbol{G}_{\mathrm{s},h}^k \underline{\boldsymbol{u}}_h) - \boldsymbol{\sigma}(\cdot, \boldsymbol{\nabla}_{\mathrm{s}} \boldsymbol{u})) : (\boldsymbol{G}_{\mathrm{s},h}^k \underline{\boldsymbol{u}}_h - \boldsymbol{\nabla}_{\mathrm{s}} \boldsymbol{u}).$$

For all $h \in \mathcal{H}$, the function $\mathcal{D}_h$ is non-negative as a result of the monotonicity property (2e) and, by (52) with $\boldsymbol{\Lambda} = \boldsymbol{\nabla}_{\mathrm{s}} \boldsymbol{u}$, it is inferred that $\lim_{h\to 0} \int_\Omega \mathcal{D}_h = 0$. Hence, $(\mathcal{D}_h)_{h\in\mathcal{H}}$ converges to 0 in $L^1(\Omega)$ and, therefore, also almost everywhere on Ω up to a subsequence. Let us take $\overline{\boldsymbol{x}} \in \Omega$ such that the above mentioned convergence hold at $\overline{\boldsymbol{x}}$. Developing the products in $\mathcal{D}_h$ and using the coercivity and growth properties (2d) and (2c) of $\boldsymbol{\sigma}$ one has

$$\mathcal{D}_h(\overline{\boldsymbol{x}}) \geqslant \underline{\sigma} \|\boldsymbol{G}_{\mathrm{s},h}^k \underline{\boldsymbol{u}}_h(\overline{\boldsymbol{x}})\|_{d\times d}^2 - 2\overline{\sigma} \|\boldsymbol{G}_{\mathrm{s},h}^k \underline{\boldsymbol{u}}_h(\overline{\boldsymbol{x}})\|_{d\times d} \|\boldsymbol{\nabla}_{\mathrm{s}} \boldsymbol{u}(\overline{\boldsymbol{x}})\|_{d\times d} + \underline{\sigma} \|\boldsymbol{\nabla}_{\mathrm{s}} \boldsymbol{u}(\overline{\boldsymbol{x}})\|_{d\times d}^2.$$

Since the right hand side is quadratic in $\|\boldsymbol{G}_{\mathrm{s},h}^k \underline{\boldsymbol{u}}_h(\overline{\boldsymbol{x}})\|_{d\times d}$ and $(\mathcal{D}_h(\overline{\boldsymbol{x}}))_{h\in\mathcal{H}}$ is bounded, we deduce that also $(\boldsymbol{G}_{\mathrm{s},h}^k \underline{\boldsymbol{u}}_h(\overline{\boldsymbol{x}}))_{h\in\mathcal{H}}$ is bounded. Passing to the limit in the definition of $\mathcal{D}_h(\overline{\boldsymbol{x}})$ yields

$$(\boldsymbol{\sigma}(\overline{\boldsymbol{x}}, \boldsymbol{L}_{\overline{\boldsymbol{x}}}) - \boldsymbol{\sigma}(\overline{\boldsymbol{x}}, \boldsymbol{\nabla}_{\mathrm{s}} \boldsymbol{u}(\overline{\boldsymbol{x}}))) : (\boldsymbol{L}_{\overline{\boldsymbol{x}}} - \boldsymbol{\nabla}_{\mathrm{s}} \boldsymbol{u}(\overline{\boldsymbol{x}})) = 0,$$

where $\boldsymbol{L}_{\overline{\boldsymbol{x}}}$ is an adherence value of $(\boldsymbol{G}_{\mathrm{s},h}^k \underline{\boldsymbol{u}}_h(\overline{\boldsymbol{x}}))_{h\in\mathcal{H}}$. The strict monotonicity assumption forces $\boldsymbol{L}_{\overline{\boldsymbol{x}}} = \boldsymbol{\nabla}_{\mathrm{s}} \boldsymbol{u}(\overline{\boldsymbol{x}})$ to be the unique adherence value of $(\boldsymbol{G}_{\mathrm{s},h}^k \underline{\boldsymbol{u}}_h(\overline{\boldsymbol{x}}))_{h\in\mathcal{H}}$ and therefore the sequence converges to this value. As a result

$$\boldsymbol{G}_{\mathrm{s},h}^k \underline{\boldsymbol{u}}_h \to \boldsymbol{\nabla}_{\mathrm{s}} \boldsymbol{u} \text{ a.e. on } \Omega. \tag{53}$$

Using (51) together with Fatou's Lemma, we see that

$$\lim_{h\to 0} \int_\Omega \boldsymbol{\sigma}(\cdot, \boldsymbol{G}_{\mathrm{s},h}^k \underline{\boldsymbol{u}}_h) : \boldsymbol{G}_{\mathrm{s},h}^k \underline{\boldsymbol{u}}_h = \int_\Omega \boldsymbol{\sigma}(\cdot, \boldsymbol{\nabla}_{\mathrm{s}} \boldsymbol{u}) : \boldsymbol{\nabla}_{\mathrm{s}} \boldsymbol{u}.$$

Moreover, owing to (53), $(\boldsymbol{\sigma}(\cdot, \boldsymbol{G}_{\mathrm{s},h}^k \underline{\boldsymbol{u}}_h) : \boldsymbol{G}_{\mathrm{s},h}^k \underline{\boldsymbol{u}}_h)_{h\in\mathcal{H}}$ is a non-negative sequence converging almost everywhere on Ω. Using [21, Lemma 8.4] we see that this sequence also converges in $L^1(\Omega)$ and, therefore, it is equi-integrable in $L^1(\Omega)$. Thus, the coercivity (2d) of $\boldsymbol{\sigma}$ ensures that $(\boldsymbol{G}_{\mathrm{s},h}^k \underline{\boldsymbol{u}}_h)_{h\in\mathcal{H}}$ is equi-integrable in $L^2(\Omega; \mathbb{R}^{d\times d})$ and Vitali's theorem shows that

$$\boldsymbol{G}_{\mathrm{s},h}^k \underline{\boldsymbol{u}}_h \to \boldsymbol{\nabla}_{\mathrm{s}} \boldsymbol{u} \text{ strongly in } L^2(\Omega; \mathbb{R}^{d\times d}). \qquad \square$$

7.3 Error estimate

Proof of Theorem 15. For the sake of conciseness, throughout the proof we let $\widehat{\underline{\boldsymbol{u}}}_h := \underline{\boldsymbol{I}}_h^k \boldsymbol{u}$ and use the following abridged notations for the constraint field and its approximations:

$$\varsigma := \boldsymbol{\sigma}(\cdot, \boldsymbol{\nabla}_{\mathrm{s}} \boldsymbol{u}) \text{ and, for all } T \in \mathcal{T}_h,\ \varsigma_T := \boldsymbol{\sigma}(\cdot, \boldsymbol{G}_{\mathrm{s},T}^k \underline{\boldsymbol{u}}_T) \text{ and } \widehat{\varsigma}_T := \boldsymbol{\sigma}(\cdot, \boldsymbol{G}_{\mathrm{s},T}^k \widehat{\underline{\boldsymbol{u}}}_T).$$

First we want to show that (31) holds assuming that

$$\|\underline{\boldsymbol{u}}_h - \widehat{\underline{\boldsymbol{u}}}_h\|_{\epsilon,h} \lesssim h^{k+1} \left(\|\boldsymbol{u}\|_{H^{k+2}(\mathcal{T}_h;\mathbb{R}^d)} + \|\varsigma\|_{H^{k+1}(\mathcal{T}_h;\mathbb{R}^{d\times d})} \right). \tag{54}$$

Using the triangle inequality, we obtain

$$\begin{aligned} \|\boldsymbol{G}_{\mathrm{s},h}^k \underline{\boldsymbol{u}}_h - \boldsymbol{\nabla}_{\mathrm{s}} \boldsymbol{u}\| + s_h(\underline{\boldsymbol{u}}_h, \underline{\boldsymbol{u}}_h)^{1/2} &\leqslant \|\boldsymbol{G}_{\mathrm{s},h}^k (\underline{\boldsymbol{u}}_h - \widehat{\underline{\boldsymbol{u}}}_h)\| + s_h(\underline{\boldsymbol{u}}_h - \widehat{\underline{\boldsymbol{u}}}_h, \underline{\boldsymbol{u}}_h - \widehat{\underline{\boldsymbol{u}}}_h)^{1/2} \\ &\quad + \|\boldsymbol{G}_{\mathrm{s},h}^k \widehat{\underline{\boldsymbol{u}}}_h - \boldsymbol{\nabla}_{\mathrm{s}} \boldsymbol{u}\| + s_h(\widehat{\underline{\boldsymbol{u}}}_h, \widehat{\underline{\boldsymbol{u}}}_h)^{1/2}. \end{aligned} \tag{55}$$

Using the norm equivalence (28) followed by (54) we obtain for the terms in the first line of (55)

$$\|\boldsymbol{G}_{\mathrm{s},h}^k (\underline{\boldsymbol{u}}_h - \widehat{\underline{\boldsymbol{u}}}_h)\| + s_h(\underline{\boldsymbol{u}}_h - \widehat{\underline{\boldsymbol{u}}}_h, \underline{\boldsymbol{u}}_h - \widehat{\underline{\boldsymbol{u}}}_h)^{1/2} \lesssim h^{k+1} \left(\|\boldsymbol{u}\|_{H^{k+2}(\mathcal{T}_h;\mathbb{R}^d)} + \|\varsigma\|_{H^{k+1}(\mathcal{T}_h;\mathbb{R}^{d\times d})} \right).$$

For the terms in the second line, using the approximation properties of $\boldsymbol{G}_{\mathrm{s},h}^k$ resulting from (18) together with (13a) for the first addend and (48) for the second, we get

$$\|\boldsymbol{G}_{\mathrm{s},h}^k \widehat{\underline{\boldsymbol{u}}}_h - \boldsymbol{\nabla}_{\mathrm{s}} \boldsymbol{u}\| + s_h(\widehat{\underline{\boldsymbol{u}}}_h, \widehat{\underline{\boldsymbol{u}}}_h)^{1/2} \lesssim h^{k+1} \|\boldsymbol{u}\|_{H^{k+2}(\mathcal{T}_h;\mathbb{R}^d)}.$$

It only remains to prove (54), which we do in two steps: in **Step 1** we prove a basic estimate in terms of a conformity error, which is then bounded in **Step 2**.

Step 1: ***Basic error estimate.*** Using for all $T \in \mathcal{T}_h$ the strong monotonicity (30b) with $\boldsymbol{\tau} = \boldsymbol{G}_{\mathrm{s},T}^k \widehat{\underline{\boldsymbol{u}}}_T$ and $\boldsymbol{\eta} = \boldsymbol{G}_{\mathrm{s},T}^k \underline{\boldsymbol{u}}_T$, we infer

$$\|\boldsymbol{G}_{\mathrm{s},h}^k(\widehat{\underline{\boldsymbol{u}}}_h - \underline{\boldsymbol{u}}_h)\|^2 \lesssim \sum_{T\in\mathcal{T}_h} \int_T (\widehat{\boldsymbol{\varsigma}}_T - \boldsymbol{\varsigma}_T) : \boldsymbol{G}_{\mathrm{s},T}^k(\widehat{\underline{\boldsymbol{u}}}_T - \underline{\boldsymbol{u}}_T).$$

Owing to the norm equivalence (28) and the previous bound, we get

$$\begin{aligned}
\|\widehat{\underline{\boldsymbol{u}}}_h - \underline{\boldsymbol{u}}_h\|_{\epsilon,h}^2 &\lesssim \sum_{T\in\mathcal{T}_h} \int_T (\widehat{\boldsymbol{\varsigma}}_T - \boldsymbol{\varsigma}_T) : \boldsymbol{G}_{\mathrm{s},T}^k(\widehat{\underline{\boldsymbol{u}}}_T - \underline{\boldsymbol{u}}_T) + s_h(\widehat{\underline{\boldsymbol{u}}}_h - \underline{\boldsymbol{u}}_h, \widehat{\underline{\boldsymbol{u}}}_h - \underline{\boldsymbol{u}}_h) \\
&= a_h(\widehat{\underline{\boldsymbol{u}}}_h, \widehat{\underline{\boldsymbol{u}}}_h - \underline{\boldsymbol{u}}_h) - \int_\Omega \boldsymbol{f} \cdot (\widehat{\underline{\boldsymbol{u}}}_h - \underline{\boldsymbol{u}}_h).
\end{aligned}$$

where we have used the discrete problem (24) to conclude. Hence, dividing by $\|\widehat{\underline{\boldsymbol{u}}}_h - \underline{\boldsymbol{u}}_h\|_{\epsilon,h}$ and passing to the supremum in the right-hand side, we arrive at the following error estimate:

$$\|\widehat{\underline{\boldsymbol{u}}}_h - \underline{\boldsymbol{u}}_h\|_{\epsilon,h} \lesssim \sup_{\underline{\boldsymbol{v}}_h \in \underline{\boldsymbol{U}}_{h,0}^k,\ \|\underline{\boldsymbol{v}}_h\|_{\epsilon,h}=1} \mathcal{E}_h(\underline{\boldsymbol{v}}_h), \tag{56}$$

with conformity error such that, for all $\underline{\boldsymbol{v}}_h \in \underline{\boldsymbol{U}}_{h,0}^k$,

$$\mathcal{E}_h(\underline{\boldsymbol{v}}_h) := \sum_{T\in\mathcal{T}_h} \int_T \widehat{\boldsymbol{\varsigma}}_T : \boldsymbol{G}_{\mathrm{s},T}^k \underline{\boldsymbol{v}}_T - \int_\Omega \boldsymbol{f} \cdot \boldsymbol{v}_h + s_h(\widehat{\underline{\boldsymbol{u}}}_h, \underline{\boldsymbol{v}}_h). \tag{57}$$

Step 2: ***Bound of the conformity error.*** We bound the quantity $\mathcal{E}_h(\underline{\boldsymbol{v}}_h)$ defined above for a generic $\underline{\boldsymbol{v}}_h \in \underline{\boldsymbol{U}}_{h,0}^k$. Denote by $\mathfrak{T}_1$, $\mathfrak{T}_2$, and $\mathfrak{T}_3$ the three addends in the right-hand side of (57).

Using for all $T \in \mathcal{T}_h$ the definition (17) of $\boldsymbol{G}_{\mathrm{s},T}^k$ with $\boldsymbol{\tau} = \boldsymbol{\pi}_T^k \widehat{\boldsymbol{\varsigma}}_T$, we have that

$$\mathfrak{T}_1 = \sum_{T\in\mathcal{T}_h} \left(\int_T \widehat{\boldsymbol{\varsigma}}_T : \boldsymbol{\nabla}_{\mathrm{s}} \boldsymbol{v}_T + \sum_{F\in\mathcal{F}_T} \int_F \boldsymbol{\pi}_T^k \widehat{\boldsymbol{\varsigma}}_T \boldsymbol{n}_{TF} \cdot (\boldsymbol{v}_F - \boldsymbol{v}_T) \right), \tag{58}$$

where we have used the fact that $\boldsymbol{\nabla}_{\mathrm{s}} \boldsymbol{v}_T \in \mathbb{P}^{k-1}(T;\mathbb{R}^{d\times d})$ together with the definition (12) of the orthogonal projector to cancel $\boldsymbol{\pi}_T^k$ in the first term.

On the other hand, using the fact that $\boldsymbol{f} = -\boldsymbol{\nabla}\cdot\boldsymbol{\varsigma}$ a.e. in Ω and integrating by parts element by element, we get that

$$\mathfrak{T}_2 = -\sum_{T\in\mathcal{T}_h} \left(\int_T \boldsymbol{\varsigma} : \boldsymbol{\nabla}_{\mathrm{s}} \boldsymbol{v}_T + \sum_{F\in\mathcal{F}_T} \int_F \boldsymbol{\varsigma} \boldsymbol{n}_{TF} \cdot (\boldsymbol{v}_F - \boldsymbol{v}_T) \right), \tag{59}$$

where we have additionally used that $\boldsymbol{\varsigma}_{|T_1} \boldsymbol{n}_{T_1F} + \boldsymbol{\varsigma}_{|T_2} \boldsymbol{n}_{T_2F} = \boldsymbol{0}$ for all interfaces $F \subset \partial T_1 \cap \partial T_2$ and that $\boldsymbol{v}_F$ vanishes on Γ (cf. (23)) to insert $\boldsymbol{v}_F$ into the second term.

Summing (58) and (59), taking absolute values, and using the Cauchy–Schwarz inequality to bound the right-hand side, we infer that

$$|\mathfrak{T}_1 + \mathfrak{T}_2| \leqslant \left(\sum_{T\in\mathcal{T}_h} \left(\|\boldsymbol{\varsigma} - \widehat{\boldsymbol{\varsigma}}_T\|_T^2 + h_T \|\boldsymbol{\varsigma} - \boldsymbol{\pi}_T^k \widehat{\boldsymbol{\varsigma}}_T\|_{\partial T}^2 \right) \right)^{1/2} \|\underline{\boldsymbol{v}}_h\|_{\epsilon,h}. \tag{60}$$

It only remains to bound the first factor. Let a mesh element $T \in \mathcal{T}_h$ be fixed. Using the Lipschitz continuity (30a) with $\boldsymbol{\tau} = \boldsymbol{G}_{\mathrm{s},T}^k \widehat{\underline{\boldsymbol{u}}}_T$ and $\boldsymbol{\eta} = \boldsymbol{\nabla}_{\mathrm{s}} \boldsymbol{u}$ and the optimal approximation properties of $\boldsymbol{G}_{\mathrm{s},T}^k \underline{\boldsymbol{I}}_T^k$ resulting from (18) together with (13a) with $m = 1$ and $s = k+2$, leads to

$$\|\boldsymbol{\varsigma} - \widehat{\boldsymbol{\varsigma}}_T\|_T \lesssim \|\boldsymbol{\nabla}_{\mathrm{s}}\boldsymbol{u} - \boldsymbol{G}_{\mathrm{s},T}^k \widehat{\underline{\boldsymbol{u}}}_T\|_T \lesssim h^{k+1} \|\boldsymbol{u}\|_{H^{k+2}(T;\mathbb{R}^d)}, \tag{61}$$

which provides an estimate for the first term inside the summation in the right-hand side of (60). To estimate the second term, we use the triangle inequality, the discrete trace inequality of [16, Lemma 1.46], and the boundedness of $\boldsymbol{\pi}_T^k$ to write

$$h_T^{1/2} \|\boldsymbol{\varsigma} - \boldsymbol{\pi}_T^k \widehat{\boldsymbol{\varsigma}}_T\|_{\partial T} \lesssim \|\boldsymbol{\pi}_T^k(\boldsymbol{\varsigma} - \widehat{\boldsymbol{\varsigma}}_T)\|_T + h_T^{1/2} \|\boldsymbol{\varsigma} - \boldsymbol{\pi}_T^k \boldsymbol{\varsigma}\|_{\partial T} \leqslant \|\boldsymbol{\varsigma} - \widehat{\boldsymbol{\varsigma}}_T\|_T + h_T^{1/2} \|\boldsymbol{\varsigma} - \boldsymbol{\pi}_T^k \boldsymbol{\varsigma}\|_{\partial T}.$$

The first term in the right-hand side is bounded by (61). For the second, using the approximation properties (13b) of $\boldsymbol{\pi}_T^k$ with $m = 0$ and $s = k+1$, we get $h_T^{1/2} \|\boldsymbol{\varsigma} - \boldsymbol{\pi}_T^k \boldsymbol{\varsigma}\|_{\partial T} \lesssim h^{k+1} \|\boldsymbol{\varsigma}\|_{H^{k+1}(T;\mathbb{R}^{d\times d})}$ so that, in conclusion,

$$h_T^{1/2} \|\boldsymbol{\varsigma} - \boldsymbol{\pi}_T^k \widehat{\boldsymbol{\varsigma}}_T\|_{\partial T} \lesssim h^{k+1} \left(\|\boldsymbol{u}\|_{H^{k+2}(T;\mathbb{R}^d)} + \|\boldsymbol{\varsigma}\|_{H^{k+1}(T;\mathbb{R}^{d\times d})} \right). \tag{62}$$

Plugging the estimates (61) and (62) into (60) finally yields

$$|\mathfrak{T}_1 + \mathfrak{T}_2| \lesssim h^{k+1} \left(\|\boldsymbol{u}\|_{H^{k+2}(\mathcal{T}_h;\mathbb{R}^d)} + \|\boldsymbol{\varsigma}\|_{H^{k+1}(\mathcal{T}_h;\mathbb{R}^{d\times d})} \right) \|\underline{\boldsymbol{v}}_h\|_{\epsilon,h}. \tag{63}$$

It only remains to bound $\mathfrak{T}_3 = s_h(\widehat{\underline{\boldsymbol{u}}}_h, \underline{\boldsymbol{v}}_h)$. Using the Cauchy–Schwarz inequality, the definition (26) of s_h, the approximation property (48) of $\boldsymbol{\Delta}_{TF}^k$, and the norm equivalence (28), we infer

$$|\mathfrak{T}_3| \lesssim \left(\sum_{T\in\mathcal{T}_h} \sum_{F\in\mathcal{F}_T} h_F^{-1} \|\boldsymbol{\Delta}_{TF}^k \widehat{\underline{\boldsymbol{u}}}_T\|_F^2 \right)^{1/2} s_h(\underline{\boldsymbol{v}}_h, \underline{\boldsymbol{v}}_h)^{1/2} \lesssim h^{k+1} \|\boldsymbol{u}\|_{H^{k+2}(\mathcal{T}_h;\mathbb{R}^d)} \|\underline{\boldsymbol{v}}_h\|_{\epsilon,h}. \tag{64}$$

Using (63) and (64), we finally get that, for all $\underline{\boldsymbol{v}}_h \in \underline{\boldsymbol{U}}_{h,0}^k$,

$$\mathcal{E}_h(\underline{\boldsymbol{v}}_h) \lesssim h^{k+1} \left(\|\boldsymbol{u}\|_{H^{k+2}(\mathcal{T}_h;\mathbb{R}^d)} + \|\boldsymbol{\varsigma}\|_{H^{k+1}(\mathcal{T}_h;\mathbb{R}^{d\times d})} \right) \|\underline{\boldsymbol{v}}_h\|_{\epsilon,h}. \tag{65}$$

Thus, using (65) to bound the right-hand side of (56), (54) follows. □

A Technical results

This appendix contains the proofs of two technical results: the approximation properties of the discrete symmetric gradient $\boldsymbol{G}_{\mathrm{s},h}^k$ stated in Proposition 7 and the discrete Korn inequality (29).

A.1 Consistency of the discrete symmetric gradient operator

Proof of Proposition 7. Throughout the proof, we write $A \lesssim B$ for $A \leqslant MB$, where $M > 0$ does not depend on h.

1) *Strong consistency.* We first assume that $\boldsymbol{v} \in H^2(\Omega;\mathbb{R}^d)$. Owing to the commuting property (18) and the approximation property (13a) with $m = 1$ and $s = 2$, it is inferred that $\|\boldsymbol{G}_{\mathrm{s},T}^k \underline{\boldsymbol{I}}_T^k \boldsymbol{v} - \boldsymbol{\nabla}_{\mathrm{s}} \boldsymbol{v}\|_T \lesssim h \|\boldsymbol{v}\|_{H^2(T;\mathbb{R}^d)}$. Squaring, summing over $T \in \mathcal{T}_h$, and taking the square root of the resulting inequality gives

$$\|\boldsymbol{G}_{\mathrm{s},h}^k \underline{\boldsymbol{I}}_h^k \boldsymbol{v} - \boldsymbol{\nabla}_{\mathrm{s}} \boldsymbol{v}\| \lesssim h \|\boldsymbol{v}\|_{H^2(\Omega;\mathbb{R}^d)}. \tag{66}$$

If $\boldsymbol{v} \in H^1(\Omega;\mathbb{R}^d)$ we reason by density, namely we take a sequence $(\boldsymbol{v}_\epsilon)_{\epsilon>0} \subset H^2(\Omega;\mathbb{R}^d)$ that converges to $\boldsymbol{v}$ in $H^1(\Omega;\mathbb{R}^d)$ as $\epsilon \to 0$ and, using twice the triangular inequality, we write

$$\|\boldsymbol{G}_{\mathrm{s},h}^k \underline{\boldsymbol{I}}_h^k \boldsymbol{v} - \boldsymbol{\nabla}_{\mathrm{s}} \boldsymbol{v}\| \leqslant \|\boldsymbol{G}_{\mathrm{s},h}^k \underline{\boldsymbol{I}}_h^k (\boldsymbol{v} - \boldsymbol{v}_\epsilon)\| + \|\boldsymbol{G}_{\mathrm{s},h}^k \underline{\boldsymbol{I}}_h^k \boldsymbol{v}_\epsilon - \boldsymbol{\nabla}_{\mathrm{s}} \boldsymbol{v}_\epsilon\| + \|\boldsymbol{\nabla}_{\mathrm{s}}(\boldsymbol{v} - \boldsymbol{v}_\epsilon)\|. \tag{67}$$

By (66), the second term in the right-hand side tends to 0 as $h \to 0$. Moreover, owing to the commuting property (18) and the H^1-boundedness of $\boldsymbol{\pi}_T^k$, one has

$$\|\boldsymbol{G}_{\mathrm{s},h}^k \underline{\boldsymbol{I}}_h^k(\boldsymbol{v}-\boldsymbol{v}_\epsilon)\| = \left(\sum_{T\in\mathcal{T}_h} \|\boldsymbol{\pi}_T^k \boldsymbol{\nabla}_{\mathrm{s}}(\boldsymbol{v}-\boldsymbol{v}_\epsilon)\|_T^2\right)^{1/2} \leqslant \left(\sum_{T\in\mathcal{T}_h} \|\boldsymbol{\nabla}_{\mathrm{s}}(\boldsymbol{v}-\boldsymbol{v}_\epsilon)\|_T^2\right)^{1/2} \leqslant \|\boldsymbol{\nabla}_{\mathrm{s}}(\boldsymbol{v}-\boldsymbol{v}_\epsilon)\|.$$

Therefore, taking the supremum limit as $h \to 0$ and then the supremum limit as $\epsilon \to 0$, concludes the proof of (20) (notice that the order in which the limits are taken is important).

2) *Sequential consistency.* In order to prove (22) we observe that, by the definitions (19) of $\boldsymbol{G}_{\mathrm{s},h}^k$ and (17b) of $\boldsymbol{G}_{\mathrm{s},T}^k$ one has, for all $\boldsymbol{\tau} \in H^1(\Omega;\mathbb{R}_{\mathrm{sym}}^{d\times d})$ and all $\underline{\boldsymbol{v}}_h \in \underline{\boldsymbol{U}}_h^k$,

$$\begin{aligned}
\int_\Omega \boldsymbol{G}_{\mathrm{s},h}^k \underline{\boldsymbol{v}}_h : \boldsymbol{\tau} &= \sum_{T\in\mathcal{T}_h} \int_T \boldsymbol{G}_{\mathrm{s},T}^k \underline{\boldsymbol{v}}_T : \boldsymbol{\tau} \\
&= \sum_{T\in\mathcal{T}_h} \int_T (\boldsymbol{G}_{\mathrm{s},T}^k \underline{\boldsymbol{v}}_T - \boldsymbol{\nabla}_{\mathrm{s}} \boldsymbol{v}_T) : (\boldsymbol{\tau} - \boldsymbol{\pi}_T^0 \boldsymbol{\tau}) + \sum_{T\in\mathcal{T}_h} \int_T (\boldsymbol{G}_{\mathrm{s},T}^k \underline{\boldsymbol{v}}_T - \boldsymbol{\nabla}_{\mathrm{s}} \boldsymbol{v}_T) : \boldsymbol{\pi}_T^0 \boldsymbol{\tau} + \sum_{T\in\mathcal{T}_h} \int_T \boldsymbol{\nabla}_{\mathrm{s}} \boldsymbol{v}_T : \boldsymbol{\tau} \\
&= \mathfrak{T}_1 + \sum_{T\in\mathcal{T}_h} \sum_{F\in\mathcal{F}_T} \int_F (\boldsymbol{v}_F - \boldsymbol{v}_T)\cdot(\boldsymbol{\pi}_T^0 \boldsymbol{\tau}) \boldsymbol{n}_{TF} + \sum_{T\in\mathcal{T}_h} \int_T \boldsymbol{\nabla}_{\mathrm{s}} \boldsymbol{v}_T : \boldsymbol{\tau} \\
&= \mathfrak{T}_1 + \sum_{T\in\mathcal{T}_h} \sum_{F\in\mathcal{F}_T} \int_F (\boldsymbol{v}_F - \boldsymbol{v}_T)\cdot(\boldsymbol{\pi}_T^0 \boldsymbol{\tau} - \boldsymbol{\tau}) \boldsymbol{n}_{TF} - \sum_{T\in\mathcal{T}_h} \int_T \boldsymbol{v}_T \cdot (\boldsymbol{\nabla}\cdot\boldsymbol{\tau}) + \sum_{F\in\mathcal{F}_h^{\mathrm{b}}} \int_F \boldsymbol{v}_F \cdot (\boldsymbol{\tau}\boldsymbol{n}_{TF}) \\
&= \mathfrak{T}_1 + \mathfrak{T}_2 - \int_\Omega \boldsymbol{v}_h \cdot (\boldsymbol{\nabla}\cdot\boldsymbol{\tau}) + \int_\Gamma \boldsymbol{v}_{\Gamma,h} \cdot \boldsymbol{\gamma}_{\boldsymbol{n}}(\boldsymbol{\tau}).
\end{aligned} \tag{68}$$

In the fourth line, we used an element-wise integration by parts together with the relation

$$\sum_{T\in\mathcal{T}_h} \sum_{F\in\mathcal{F}_T\cap\mathcal{F}_h^{\mathrm{i}}} \int_F \boldsymbol{v}_F \cdot (\boldsymbol{\tau}\boldsymbol{n}_{TF}) = \sum_{F\in\mathcal{F}_h^{\mathrm{i}}} \int_F \boldsymbol{v}_F \cdot (\boldsymbol{\tau}\boldsymbol{n}_{T_1F} + \boldsymbol{\tau}\boldsymbol{n}_{T_2F}) = 0,$$

where for all $F \in \mathcal{F}_h^{\mathrm{i}}$, $T_1, T_2 \in \mathcal{T}_h$ are such that $F \subset \partial T_1 \cap \partial T_2$. Owing to (68), the conclusion follows once we prove that $|\mathfrak{T}_1 + \mathfrak{T}_2| \lesssim h\|\underline{\boldsymbol{v}}_h\|_{\epsilon,h}\|\boldsymbol{\tau}\|_{H^1(\Omega;\mathbb{R}^{d\times d})}$. By (13a) (with $m=0$ and $s=1$) we have $\|\boldsymbol{\tau}-\boldsymbol{\pi}_T^0\boldsymbol{\tau}\|_T \lesssim h_T\|\boldsymbol{\tau}\|_{H^1(T;\mathbb{R}^{d\times d})}$ and thus, using the Cauchy–Schwarz and triangle inequalities followed by the norm equivalence (28),

$$\begin{aligned}
|\mathfrak{T}_1| &\leqslant \left(\sum_{T\in\mathcal{T}_h} \|\boldsymbol{G}_{\mathrm{s},T}^k \underline{\boldsymbol{v}}_T - \boldsymbol{\nabla}_{\mathrm{s}} \boldsymbol{v}_T\|_T^2\right)^{1/2} \left(\sum_{T\in\mathcal{T}_h} \|\boldsymbol{\tau}-\boldsymbol{\pi}_T^0\boldsymbol{\tau}\|_T^2\right)^{1/2} \\
&\lesssim h\left(\|\boldsymbol{G}_{\mathrm{s},h}^k \underline{\boldsymbol{v}}_h\|^2 + \|\underline{\boldsymbol{v}}_h\|_{\epsilon,h}^2\right)^{1/2} \|\boldsymbol{\tau}\|_{H^1(\Omega;\mathbb{R}^{d\times d})} \lesssim h\|\underline{\boldsymbol{v}}_h\|_{\epsilon,h}\|\boldsymbol{\tau}\|_{H^1(\Omega;\mathbb{R}^{d\times d})}.
\end{aligned} \tag{69}$$

In a similar way, we obtain an upper bound for $\mathfrak{T}_2$. By (13b) (with $m=0$ and $s=1$), for all $F \in \mathcal{F}_T$, we have $\|\boldsymbol{\tau}-\boldsymbol{\pi}_T^0\boldsymbol{\tau}\|_F \lesssim h_T^{1/2}\|\boldsymbol{\tau}\|_{H^1(T;\mathbb{R}^{d\times d})} \lesssim h_F^{1/2}\|\boldsymbol{\tau}\|_{H^1(T;\mathbb{R}^{d\times d})}$ and thus, using the Cauchy–Schwarz inequality,

$$|\mathfrak{T}_2| \lesssim \sum_{T\in\mathcal{T}_h} \sum_{F\in\mathcal{F}_T} h_F^{1/2} \|\boldsymbol{v}_F - \boldsymbol{v}_T\|_F \|\boldsymbol{\tau}\|_{H^1(T;\mathbb{R}^{d\times d})} \lesssim h\|\underline{\boldsymbol{v}}_h\|_{\epsilon,h}\|\boldsymbol{\tau}\|_{H^1(\Omega;\mathbb{R}^{d\times d})}. \tag{70}$$

Owing to (69) and (70), the triangle inequality $|\mathfrak{T}_1 + \mathfrak{T}_2| \leqslant |\mathfrak{T}_1| + |\mathfrak{T}_2|$ yields the conclusion. □

A.2 A discrete Korn inequality

Proposition 19 (Discrete Korn inequality)**.** *Assume that the mesh further verifies the assumption of [7, Theorem 4.2] if $d = 2$ and [7, Theorem 5.2] if $d = 3$. Then, the discrete Korn inequality (29) holds.*

Proof. Using the broken Korn inequality [7, Eq. (1.22)] on $H^1(\mathcal{T}_h;\mathbb{R}^d)$ followed by the Cauchy–Schwarz inequality, one has

$$\begin{aligned}\|\boldsymbol{v}_h\|^2+\|\boldsymbol{\nabla}_h\boldsymbol{v}_h\|^2 &\lesssim \|\boldsymbol{\nabla}_{\mathrm{s},h}\boldsymbol{v}_h\|^2+\sum_{F\in\mathcal{F}_h^{\mathrm{i}}} h_F^{-1}\|[\boldsymbol{v}_h]_F\|_F^2+\sup_{\boldsymbol{m}\in\mathbb{P}^1(\mathcal{T}_h;\mathbb{R}^d),\,\|\boldsymbol{\gamma_n}(\boldsymbol{m})\|_\Gamma=1}\left(\int_\Gamma \boldsymbol{\gamma}(\boldsymbol{v}_h)\cdot\boldsymbol{\gamma_n}(\boldsymbol{m})\right)^2\\ &\lesssim \|\boldsymbol{\nabla}_{\mathrm{s},h}\boldsymbol{v}_h\|^2+\sum_{F\in\mathcal{F}_h^{\mathrm{i}}} h_F^{-1}\|[\boldsymbol{v}_h]_F\|_F^2+\sum_{F\in\mathcal{F}_h^{\mathrm{b}}}\|\boldsymbol{v}_{h|F}\|_F^2.\end{aligned} \tag{71}$$

For an interface $F\in\mathcal{F}_{T_1}\cap\mathcal{F}_{T_2}$, we have introduced the jump $[\boldsymbol{v}_h]_F:=\boldsymbol{v}_{T_1}-\boldsymbol{v}_{T_2}$. Thus, using the triangle inequality, we get $\|[\boldsymbol{v}_h]_F\|_F\leqslant\|\boldsymbol{v}_F-\boldsymbol{v}_{T_1}\|_F+\|\boldsymbol{v}_F-\boldsymbol{v}_{T_2}\|_F$. For a boundary face $F\in\mathcal{F}_h^{\mathrm{b}}$ such that $F\in\mathcal{F}_T\cap\mathcal{F}_h^{\mathrm{b}}$ for some $T\in\mathcal{T}_h$ we have, on the other hand, $\|\boldsymbol{v}_{h|F}\|_F=\|\boldsymbol{v}_F-\boldsymbol{v}_T\|_F$ since $\boldsymbol{v}_F\equiv 0$ (cf. (23)). Using these relations in the right-hand side of (71) and rearranging the sums leads to

$$\begin{aligned}\|\boldsymbol{v}_h\|^2+\|\boldsymbol{\nabla}_h\boldsymbol{v}_h\|^2 &\lesssim \sum_{T\in\mathcal{T}_h}\left(\|\boldsymbol{\nabla}_{\mathrm{s}}\boldsymbol{v}_T\|_T^2+\sum_{F\in\mathcal{F}_T\cap\mathcal{F}_h^{\mathrm{i}}} h_F^{-1}\|\boldsymbol{v}_F-\boldsymbol{v}_T\|_F^2\right)+h\sum_{F\in\mathcal{F}_h^{\mathrm{b}}} h_F^{-1}\|\boldsymbol{v}_F-\boldsymbol{v}_{h|F}\|_F^2\\ &\lesssim \max\{1,d_\Omega\}\sum_{T\in\mathcal{T}_h}\left(\|\boldsymbol{\nabla}_{\mathrm{s}}\boldsymbol{v}_T\|_T^2+\sum_{F\in\mathcal{F}_T} h_F^{-1}\|\boldsymbol{v}_F-\boldsymbol{v}_T\|_F^2\right),\end{aligned}$$

where d_Ω denotes the diameter of Ω. Owing to the definition (14) of the discrete strain seminorm, the latter yields the assertion. □

References

[1] A. M. Barrientos, N. G. Gatica, and P. E. Stephan. A mixed finite element method for nonlinear elasticity: two-fold saddle point approach and a-posteriori error estimate. *Numer. Math.*, 91(2):197–222, 2002.

[2] F. Bassi, L. Botti, A. Colombo, D. A. Di Pietro, and P. Tesini. On the flexibility of agglomeration based physical space discontinuous Galerkin discretizations. *J. Comput. Phys.*, 231(1):45–65, 2012.

[3] L. Beirão da Veiga, F. Brezzi, and L. D. Marini. Virtual elements for linear elasticity problems. *SIAM J. Numer. Anal.*, 2(51):794–812, 2013.

[4] L. Beirão da Veiga, C. Lovadina, and D. Mora. A virtual element method for elastic and inelastic problems on polytope meshes. *Comput. Methods Appl. Mech. Engrg.*, 295:327–346, 2015.

[5] C. Bi and Y. Lin. Discontinuous Galerkin method for monotone nonlinear elliptic problems. *Int. J. Numer. Anal. Model*, 9:999–1024, 2012.

[6] S.O.R. Biabanaki, A.R. Khoei, and P. Wriggers. Polygonal finite element methods for contact-impact problems on non-conformal meshes. *Comput. Meth. Appl. Mech. Engrg.*, 269:198–221, 2014.

[7] S. C. Brenner. Korn's inequalities for piecewise H^1 vector fields. *Math. Comp.*, 73(247):1067–1087, 2004.

[8] H. Brezis. *Functional Analysis, Sobolev Spaces and Partial Differential Equations.* Universitext. Springer New York, 2010.

[9] M. Cervera, M. Chiumenti, and R. Codina. Mixed stabilized finite element methods in nonlinear solid mechanics: Part II: Strain localization. *Comput. Methods in Appl. Mech. and Engrg.*, 199(37–40):2571–2589, 2010.

[10] H. Chi, C. Talischi, O. Lopez-Pamies, and G. H. Paulino. Polygonal finite elements for finite elasticity. *Int. J. Numer. Methods Eng.*, 101(4):305–328, 2015.

[11] K. Deimling. Nonlinear functional analysis. *Springer-Verlag, Berlin*, 1985.

[12] M. Destrade and R. W. Ogden. On the third- and fourth-order constants of incompressible isotropic elasticity. *The Journal of the Acoustical Society of America*, 128(6):3334–3343, 2010.

[13] D. A. Di Pietro and J. Droniou. A Hybrid High-Order method for Leray–Lions elliptic equations on general meshes. *Math. Comp.*, 2016. Published online.

[14] D. A. Di Pietro and J. Droniou. $W^{s,p}$-approximation properties of elliptic projectors on polynomial spaces, with application to the error analysis of a Hybrid High-Order discretisation of Leray–Lions problems. Preprint arXiv 1606.02832 [math.NA], June 2016.

[15] D. A. Di Pietro, J. Droniou, and A. Ern. A discontinuous-skeletal method for advection-diffusion-reaction on general meshes. *SIAM J. Numer. Anal.*, 53(5):2135–2157, 2015.

[16] D. A. Di Pietro and A. Ern. *Mathematical aspects of discontinuous Galerkin methods*, volume 69 of *Mathématiques & Applications.* Springer-Verlag, Berlin, 2012.

[17] D. A. Di Pietro and A. Ern. A hybrid high-order locking-free method for linear elasticity on general meshes. *Comput. Meth. Appl. Mech. Engrg.*, 283:1–21, 2015.

[18] D. A. Di Pietro and S. Lemaire. An extension of the Crouzeix–Raviart space to general meshes with application to quasi-incompressible linear elasticity and Stokes flow. *Math. Comp.*, 84(291):1–31, 2015.

[19] D. A. Di Pietro and S. Nicaise. A locking-free discontinuous Galerkin method for linear elasticity in locally nearly incompressible heterogeneous media. *Appl. Numer. Math.*, 63:105 – 116, 2013.

[20] D. A. Di Pietro and R. Specogna. An a posteriori-driven adaptive Mixed High-Order method with application to electrostatics. *J. Comput. Phys.*, 326(1):35–55, 2016.

[21] J. Droniou. Finite volume schemes for fully non-linear elliptic equations in divergence form. *ESAIM: Mathematical Modelling and Numerical Analysis*, 40(6):1069–1100, 2006.

[22] J. Droniou, R. Eymard, T. Gallouët, C. Guichard, and R. Herbin. The gradient discretisation method, November 2016. Preprint hal-01366646.

[23] J. Droniou and B. P. Lamichhane. Gradient schemes for linear and non-linear elasticity equations. *Numer. Math.*, 129(2):251–277, February 2015.

[24] G. Duvaut and Lions J.L. *Inequalities in Mechanics and Physics*. Grundlehren der mathematischen Wissenschaften 219. Springer-Verlag Berlin Heidelberg, 1 edition, 1976.

[25] L. C. Evans and R. F. Gariepy. *Measure theory and fine properties of functions*. Studies in advanced mathematics. CRC Press, Boca Raton (Fla.), 1992.

[26] G. N. Gatica, A. Márquez, and W. Rudolph. A priori and a posteriori error analyses of augmented twofold saddle point formulations for nonlinear elasticity problems. *Comput. Meth. Appl. Mech. Engrg.*, 264:23–48, 2013.

[27] G. N. Gatica and E. P. Stephan. A mixed-FEM formulation for nonlinear incompressible elasticity in the plane. *Numer. Methods Partial Differ. Equ.*, 18(1):105–128, 2002.

[28] G. N. Gatica and W. L. Wendland. Coupling of mixed finite elements and boundary elements for a hyperelastic interface problem. *SIAM J. on Numer. Anal.*, 34(6):2335–2356, 1997.

[29] R. Herbin and F. Hubert. Benchmark on discretization schemes for anisotropic diffusion problems on general grids. In R. Eymard and J.-M. Hérard, editors, *Finite Volumes for Complex Applications V*, pages 659–692. John Wiley & Sons, 2008.

[30] D. S. Hughes and J. L. Kelly. Second-order elastic deformation of solids. *Phys. Rev.*, 92:1145–1149, 1953.

[31] L. D. Landau and E. M. Lifshitz. *Theory of elasticity*. Pergamon London, 1959.

[32] S. E. Leon, D. W. Spring, and G. H. Paulino. Reduction in mesh bias for dynamic fracture using adaptive splitting of polygonal finite elements. *Int. J. Numer. Methods Eng.*, 100(8):555–576, 2014.

[33] G. J. Minty. On a "monotonicity" method for the solution of nonlinear equations in banach spaces. *Proceedings of the National Academy of Sciences of the United States of America*, 50(6):1038–1041, 1963.

[34] J. Nečas. *Introduction to the theory of nonlinear elliptic equations*. A Wiley-Interscience Publication. John Wiley & Sons Ltd., Chichester, 1986. Reprint of the 1983 edition.

[35] C. Ortner and E. Süli. Discontinuous Galerkin finite element approximation of nonlinear second-order elliptic and hyperbolic systems. *SIAM J. on Numer. Anal.*, 45(4):1370–1397, 2007.

[36] M. Pitteri and G. Zanotto. *Continuum models for phase transitions and twinning in crystals*. Chapman & Hall/CRC, 2003.

[37] S.-C. Soon, B. Cockburn, and H. K. Stolarski. A hybridizable discontinuous Galerkin method for linear elasticity. *Internat. J. Numer. Methods Engrg.*, 80(8):1058–1092, 2009.

[38] D. W. Spring, S. E. Leon, and G. H. Paulino. Unstructured polygonal meshes with adaptive refinement for the numerical simulation of dynamic cohesive fracture. *Int. J. Fracture*, 189(1):33–57, 2014.

[39] C. Talischi, G. H. Paulino, A. Pereira, and I. F. M. Menezes. Polymesher: a general-purpose mesh generator for polygonal elements written in Matlab. *Structural and Multidisciplinary Optimization*, 45(3):309–328, 2012.

[40] L. R. G. Treolar. *The Physics of Rubber Elasticity*. Oxford: Clarendon Press, 1975.

[41] P. Wriggers, W. T. Rust, and B. D. Reddy. A virtual element method for contact. *Computational Mechanics*, 58(6):1039–1050, 2016.